JGR Atmospheres

RESEARCH ARTICLE
10.1029/2021JD034814

Direct Radiative Effects in Haboobs

J. Bukowski[1] **and S. C. van den Heever**[1]

[1]Department of Atmospheric Science, Colorado State University, Fort Collins, CO, USA

Key Points:

- Daytime dust scattering leads to colder, stronger density currents with higher windspeeds and dust emissions
- In the evening, longwave dust absorption leads to a warmer surface and warmer, weaker cold pools with suppressed winds and dust emissions
- At night, dust absorption leads to less stable and warmer cold pools with higher windspeeds, turbulence, and dust emissions

Supporting Information:

Supporting Information may be found in the online version of this article.

Correspondence to:

J. Bukowski,
jennie.bukowski@colostate.edu

Citation:

Bukowski, J., & van den Heever, S. C. (2021). Direct radiative effects in haboobs. *Journal of Geophysical Research: Atmospheres*, *126*, e2021JD034814. https://doi.org/10.1029/2021JD034814

Received 23 FEB 2021
Accepted 14 AUG 2021

Author Contributions:

Conceptualization: J. Bukowski, S. C. van den Heever
Data curation: J. Bukowski
Formal analysis: J. Bukowski
Funding acquisition: S. C. van den Heever
Investigation: J. Bukowski
Methodology: J. Bukowski, S. C. van den Heever
Project Administration: S. C. van den Heever
Resources: S. C. van den Heever
Supervision: S. C. van den Heever
Visualization: J. Bukowski
Writing – original draft: J. Bukowski
Writing – review & editing: J. Bukowski, S. C. van den Heever

Abstract Convective dust storms, or haboobs, form when strong surface winds loft loose soils in convective storm outflow boundaries. Haboobs are a public safety hazard and can cause a near instantaneous loss of visibility, inimical air quality, and contribute significantly to regional dust and radiation budgets. Nevertheless, reliable predictions of convective dust events are inhibited by a lack of understanding regarding the complex and non-linear interactions between density currents, or convective cold pools, and dust radiative effects. In this study, the Weather Research and Forecasting model coupled with Chemistry (WRF-Chem) is utilized to simulate the effect dust radiation interactions have on a long-lived haboob case study that spans three distinct radiative regimes: day (high shortwave), evening (low shortwave), and night [longwave (LW) only]. A sophisticated algorithm is used to track and identify the numerous convective old pool boundaries in the simulations and assemble statistics that represent the impact of dust radiative effects. To first order, dust scattering of shortwave radiation in the day leads to a colder, dustier, and faster moving convective cold pool. In the transition period of early evening, the shortwave effects diminish while LW dust absorption leads to warmer, slower density currents that loft less dust as they propagate. At night, the haboob is again warmer due to dust absorption, but gustier in the more stable nocturnal surface layer, leading to enhanced dust emissions.

Plain Language Summary When rain evaporates below clouds in a thunderstorm, it can produce strong, cold winds at the surface. If the surface is dry and contains loose soils, these strong winds can lift dust into the air, and create a dangerous type of dust storm called a "haboob." The dust inside a haboob can be a safety hazard, but is also a critical contributor to marine ecosystem fertilization, hurricane formation, and the Earth's climate because dust redirects and absorbs incoming energy from both the sun above and the Earth below. Depending on how dust interacts with this energy, it can have opposite effects and either warm or cool the air around it. Therefore, the strong, cold winds from the thunderstorm that created the haboob in the first place can become either colder (stronger, faster) or warmer (weaker, slower). When forecasting and issuing warnings to the public, it is important to know the strength of the haboob and how fast it will move. This study investigates when and how the dust inside a haboob can cool the dust storm and make it stronger, versus when the dust will warm the dust storm and make it weaker.

1. Introduction

Mineral dust is lofted from the surface to the atmosphere by strong winds, with the most dramatic and dangerous instance of this occurring in convective dust storms, whereby visibility can be reduced to near zero in a matter of seconds (Chen & Fryrear, 2002; Leys et al., 2011; Zhang & Wang, 1997). Convective dust storms result from dust lofting in and at the outflow boundary of a convective cold pool, a specific type of atmospheric density current which forms as precipitation evaporates and ice melts below the cloud base of a mature convective cell or convective system. The air, now cooler and denser than its surroundings, is negatively buoyant and sinks until it hits the ground, spreading out as a distinct air mass. Convective downdrafts can produce intense surface winds and depending on the soil type and moisture content, they can loft loose soils into the air (Cowie et al., 2015; Huang et al., 2018; Knippertz & Todd, 2012; Membery, 1985; Pantillon et al., 2015, 2016; Roberts & Knippertz, 2012) and produce a hazardous wall of dust known as a haboob.

Convective dust storms are a safety hazard (Middleton & Kang, 2017; Sprigg, 2016) due to the near instantaneous loss of visibility in the transportation sector (Baddock et al., 2013) and respiratory effects of inhaling particulate matter (Goudie, 2014; Middleton & Kang, 2017). Despite the immediate threat of dust storms residing on the mesoscale (~100 km), the influence of haboobs extends much further: they comprise upwards

of 30%–40% of the regional dust budget (Heinold et al., 2013; Miller et al., 2008; Pantillon et al., 2015) and can be remarkably long-lived, having been observed to travel over 1,000 km as an unambiguous entity (Flamant et al., 2007; Miller et al., 2008; Roberts & Knippertz, 2014).

Convectively generated dust storms pose a direct threat to human safety and play an important role in the earth system, yet our knowledge of the physical mechanisms controlling this phenomenon is incomplete; Uncertainties and insufficiencies in the theory and numerical representation of cold pool dynamics and aerosol feedbacks proliferate, making the research and forecasting of haboobs an unresolved challenge (Knippertz & Todd, 2012; Largeron et al., 2015; Pope et al., 2016). This study serves as a first step in comprehending the feedbacks between cold pool properties and airborne mineral dust particulates inside a haboob at the process-level by singling out one of the three aerosol feedback mechanisms: the direct aerosol radiative effect. *This study will identify how dust interacts with longwave (LW) and shortwave (SW) radiation to modify cold pool and dust storm intensity during different times of the day*.

The direct aerosol effect encompasses feedbacks from mineral dust interactions with radiation. Dust scatters and absorbs in both the solar SW and terrestrial LW parts of the electromagnetic spectrum, extinguishing and redirecting incoming and outgoing radiation in the process. Because dust modulates the earth's radiation budget and climate, many previous studies concentrated on quantifying the vertical heating and cooling rates due to absorption and scattering from both observations (Banks et al., 2014; Heintzenberg, 2009; Mishra et al., 2014) and radiative transfer modeling (Carlson & Benjamin, 1980; Lemaître et al., 2010; Meloni et al., 2015; Peris-Ferrús et al., 2017; Quijano et al., 2000). Regardless of the vertical location of a dust layer, during the day dust scatters incoming solar SW radiation and decreases net insolation at the surface, leading to a decrease in surface temperature.

Complicating matters, in addition to SW scattering, dust also absorbs in the SW and LW, emitting infrared radiation and heating the atmosphere throughout the dusty layer which, when vertically integrated, can have an opposite response of near-equal magnitude to that observed at the surface (Alamirew et al., 2018; Hansell et al., 2010; Marsham et al., 2016; Slingo et al., 2006). The combined effect of cooling at the surface and heating aloft is to decrease the atmospheric lapse rate and increase static stability in the low-levels, priming the atmosphere to resist vertical convective motions within the dusty region. Interestingly, Chen et al. (1995) studied the effect of aerosol radiation on a dusty cold front and found that surface cooling with warming aloft led to enhanced frontogenesis and vertical motions at the frontal boundary due to enhanced horizontal and vertical temperature gradients. Additionally, these changes to the thermodynamic profile alter the amount of convective available potential energy, convective inhibition, and the probability of initiating new convection along cold pool boundaries.

Concurrently, as surface temperatures decrease during the day due to the presence of dust, sensible heat fluxes (SHFs) from the ground to the air are diminished (Alamirew et al., 2018; Fan et al., 2008; Heinold et al., 2007; Jiang & Feingold, 2006; Mallet et al., 2009; Miller et al., 2004; Pérez et al., 2006; Saleeby et al., 2019) and turbulent kinetic energy (TKE) is suppressed, thereby further enhancing atmospheric stability. A reduction in TKE points fundamentally to reduced vertical mixing, reduced downward transport of momentum and less intense near-surface winds. Several modeling studies have investigated changes to the structure of the planetary boundary layer (PBL) due to the mineral dust direct effect, showing that scattering aerosol (Jacobson & Kaufman, 2006) or a dusty near-surface layer reduces TKE and increase atmospheric stability during the daytime (Barbaro et al., 2013; Bukowski & van den Heever, 2020; Chen et al., 2017; Miller et al., 2004; Perlwitz et al., 2001). Previous work has involved modeling TKE due to the dust radiative effect on low level jets, near-surface wind speeds (Alizadeh Choobari et al., 2013; Heinold et al., 2008; Jacobson & Kaufman, 2006), and cold fronts (Rémy et al., 2015), but there is not always agreement on the sign of the response and these mechanisms are unclear in the case of convective outflow boundaries.

Daytime radiative effects in dusty environments have been the focus of most previous studies, while the longwave-only nighttime regime has received relatively less attention outside of low level jets, with those studies identifying warming at night, or less efficient cooling of the nocturnal boundary layer (e.g., Mallet et al., 2009; Marsham et al., 2016; Miller et al., 2004; Saleeby et al., 2019). This nighttime effect could increase SHFs and TKE (Liu et al., 2016; Miller et al., 2004) or have little effect (Saleeby et al., 2019). As convective cold pools age into the evening, they can decouple from the surface and resemble a nocturnal

low level jet, which subsequently may affect momentum mixing and dust uplift the next morning (Heinold et al., 2013; Roberts & Knippertz, 2014). Notably, the complicated evening transition between a SW-dominated to a LW-dominated regime has been understudied in the literature. Considering that haboobs can be exceptionally long-lived (Flamant et al., 2007; Miller et al., 2008; Roberts & Knippertz, 2014) and that continental convective storms often initialize in the late afternoon to early evening (Heinold et al., 2013), the response of these interim cases is anticipated to be less straightforward than those distinctly centered in one radiative regime.

Independent of their potential to loft and transport aerosol species, convective cold pools (hereafter simply referred to as "cold pools") are an important component of weather and remain an active topic in research: cold pools transport momentum and thermodynamic perturbations, producing vigorous surface winds in the process (Vescio & Johnson, 1992). Moreover, cold pools can sustain squall line thunderstorms (Rotunno et al., 1988; Thorpe et al., 1982; Weisman & Rotunno, 2004) and initiate convection through forced ascent at their leading edge (Moncrieff & Liu, 1999; Purdom, 1982; Weaver & Nelson, 1982; Wilson & Schreiber, 1986; Tompkins, 2001; Torri et al., 2015). Cold pools also play an important role in the lofting of environmental dust into deep convection, and pathways of transporting dust from within cold pools to the updrafts have also been explored (Takemi, 2005; Tulet et al.; 2010; Seigel & van den Heever, 2012a), as has the indirect connection between dust, cloud microphysics, and cold pools (Grant & van den Heever, 2015; Knippertz et al., 2009; Seigel et al., 2013; van den Heever et al., 2006).

Prior research has also investigated the connection between pristine density currents and the land surface, including soil moisture (Drager et al., 2020; Fast et al., 2019) and surface heat fluxes (Bryan & Rotunno, 2014; Drager & van den Heever, 2017; Gentine et al., 2016; Grant & van den Heever, 2016, 2018; Kurowski et al., 2018). Both surface heat fluxes and TKE play an important role in cold pool dissipation rates and therefore any changes to these quantities due to the dust direct effect will alter cold pool lifetimes. Furthermore, the impacts of static stability on cold pool depth and intensity (Liu & Moncrieff, 2000; Seigel & van den Heever, 2012b) could also be altered by dust in and around a haboob. The higher order feedbacks due to a potential dust radiative effect on stability, SHFs, and TKE will alter mixing and entrainment of environmental air into the haboob, further modifying cold pool intensity, lifetime, and dust emissions in an abstruse way.

The dust raised by haboobs is largely contained within the convective cold pool air. The presence of these dust particles can in turn modify the dynamics of the cold pool through the radiative processes discussed above. Thus, haboobs are a unique variety of density current in that dynamically loft copious amounts of dust into themselves, simultaneously spawning particles and responding to their presence. In essence, haboobs induce their own aerosol feedbacks. Because of this added complexity of aerosol interactions, most previous research has focused on understanding either pristine cold pool dynamics or direct dust radiative effects separately, making literature combining the two sparse. Few studies have investigated how dust inside a haboob feeds back on the parent cold pool dynamics, let alone the evolution of radiative aerosol perturbations throughout the density current lifecycle through a SW, LW, and SW/LW intermediate environment. Here, we seek to quantify the direct radiative effect inside a haboob on convective cold pool properties, strength, and feedbacks on dust emissions and deposition. In order to understand this phenomenon, we will revisit an Arabian Peninsula dust event from Bukowski and van den Heever (2020) and simulate a convective dust storm with multiple interacting cold pools. All information required to reproduce these simulations and data within the manuscript are stored here: http://dx.doi.org/10.25675/10217/233939.

2. Case Study, Model, and Analysis Methods

2.1. Case Study Overview

An overview of the large-scale environment across the Arabian Peninsula for this case study can be found in Bukowski and van den Heever (2020) (hereafter BvdH20). This highly researched dust event was featured in a special issue publication, with an overview of the project, case study meteorology, and comparisons to observations found in Miller et al. (2019), and additional model/observation evaluations of dust AOD presented in Saleeby et al. (2019). However, the focus here is less on the larger-scale dust conditions from BvdH20, but on a subset of the domain and case study from August 2 that allows convection to develop. The

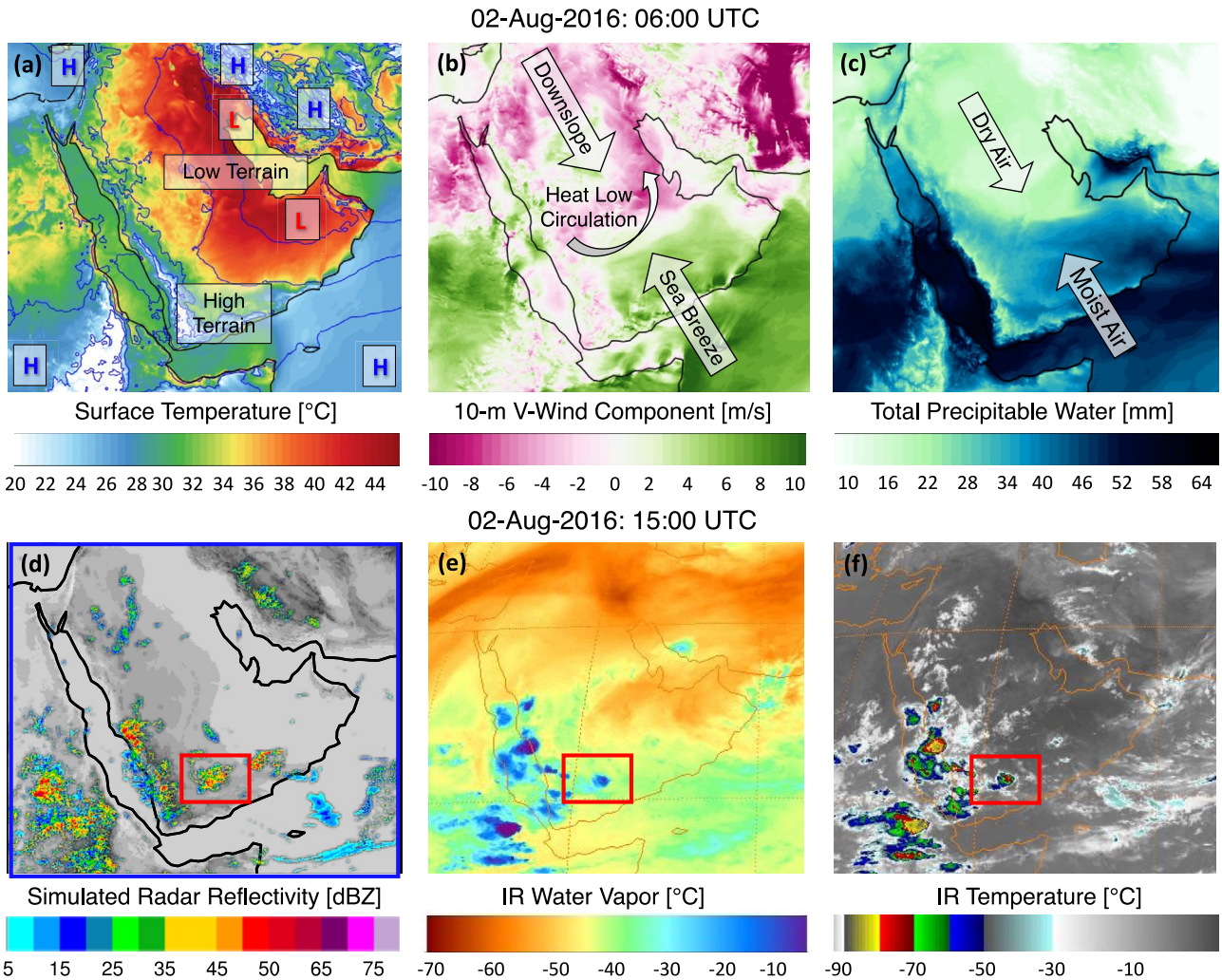

Figure 1. (Top)—Pre-storm case study meteorology setup for August 2, 2016 at 06:00 UTC from the 5-km Weather Research and Forecasting model coupled with Chemistry (WRF-Chem) radiation (RAD) simulation: (a) surface temperature and relative low and high pressure regions, (b) 10-m V wind component, (c) total precipitable water (Bottom)—Snapshot of the convective storm at August 2, 2016 at 15:00 UTC: (d) simulated radar reflectivity from the 5-km WRF-Chem RAD simulation, (e) IR water vapor temperature and (f) IR temperature from METEOSAT-7. The red boxes indicate the location of the 1.7-km inner-nest (Figure S1).

convective setup includes a sea-breeze (Figure 1b), aided by a heat low in the interior of the peninsula near Kuwait and a heat low along the Persian Gulf (Figure 1a), moving humid air (Figure 1c) from the ocean and Gulf inland. This moist air meets downslope winds from northern Saudi Arabia and Iraq moving toward the heat lows, thereby producing a convergence line. Along this line, aided by coastal topography, several pockets of convection initiate during the local afternoon around 09:00:00 UTC (12:00:00 Local), developing through the afternoon and evening (Figures 1d–1f). One of these convective clusters was chosen for the fine grid simulations, designated by the red boxes in Figure 1 and S1. This storm was selected because it is located far enough from steep terrain that orographic forcing does not unnecessarily confound the analysis, and is relatively isolated compared to other storms in the domain. Additionally, the storm system initializes in the drier interior region where dust can be expected to loft, representative of a haboob-conducive environment.

The genesis and progression of the convective system is shown throughout Figures 1–3. Convection develops as a linear feature along the convergence line and is comprised of numerous cells (Figures 2a and 2d) each producing cold pools, evident by their signature circular divergent surface winds (Figure 2g). Strong winds inside the density currents loft dust (Figure 2j), with especially high concentrations at and behind

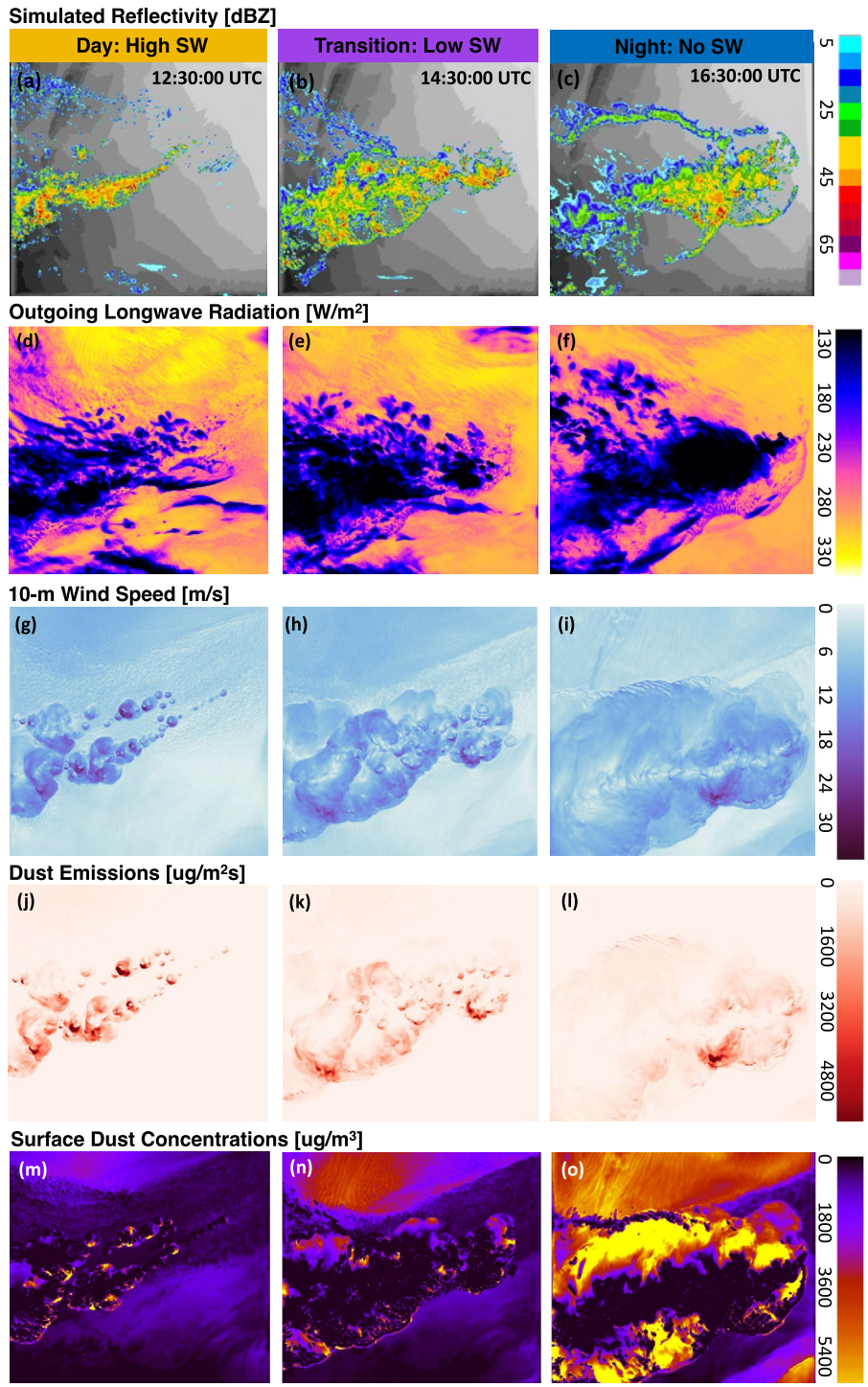

Figure 2. Dust storm progression during the three analysis time periods (day, transition, night) for the RAD simulation: (a)–(c) simulated radar reflectivity (d)–(f) outgoing longwave radiation, (g)–(i) 10-m windspeed, (j)–(l) dust emission rate, and (m)–(o) surface dust concentrations.

gust front boundaries (Figure 2m). As the storm develops, convective cells and cold pools interact to form a more unified convective complex, where discrete cells and individual cold pools become difficult to identify (Figure 2—center column). In the mature phase of the storm's lifetime, a clear, collective gust front is visible north and south of the convective line, with sufficient vertical motion at the outflow boundary to produce

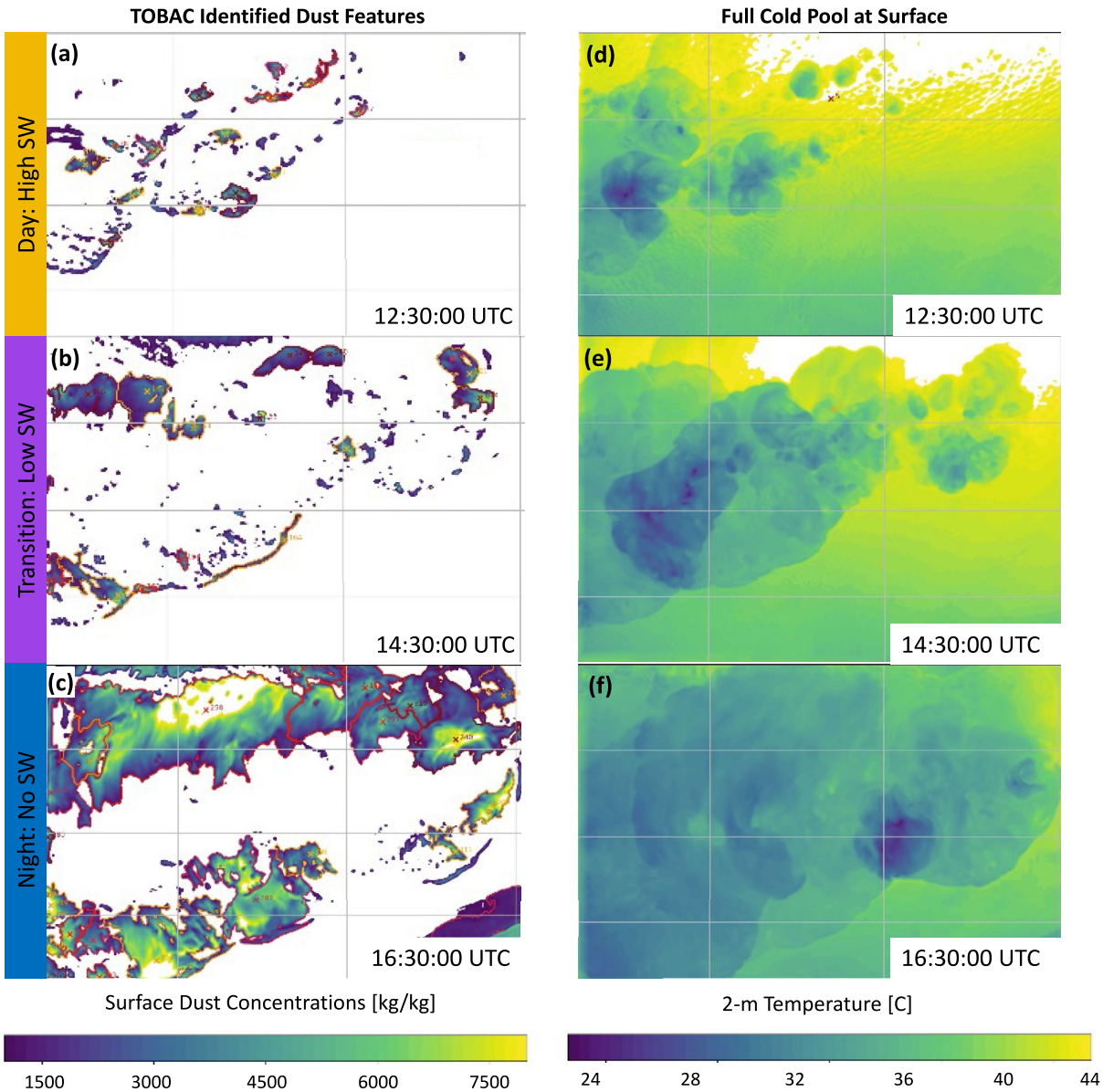

Figure 3. (Left)—Outlines of Tracking and Object-Based Analysis of Clouds-identified dust-laden boundaries (red lines) layered over surface dust concentrations for the three analysis times (day, transition, night) from the RAD simulation. Outlines represent only the dusty parts of the cold pool, with the threshold weighted center of each figure marked with and "X." (Right)—2-m temperature for the three analysis times. The right-side panels represent the full outflow boundary.

light precipitation (Figure 2c) that scavenges dust (Figure 2o). In later time periods, the location of maximum dust concentrations correlates with the maximum wind speed behind the gust front (Figure 2—right column).

It is important to note that while the storm and airborne dust concentrations develop, there is a simultaneous change in radiation occurring, both in response to the diurnal cycle and the lofting of dust. The initiation of the storm lifecycle occurs under a daytime SW-dominated regime, while strengthening takes place during a SW to LW transition in the early evening, reaching a mature storm phase in a LW-only regime at night (Section 2.4.1). It is impossible to deconvolve the radiation and storm lifecycle as they are both being perturbed concurrently. This is a limitation of the case study and warrants future study.

2.2. WRF-Chem Model Description

For consistency, the setup and parameterizations are almost identical to that used in BvdH20 including WRF-Chem version 3.9.1.1 (Fast et al., 2006; Grell et al., 2005; Skamarock et al., 2008) coupled to the GOCART module (Ginoux et al., 2001) and initialized with the same boundary conditions from the GDAS-FNL database (National Centers for Environmental Prediction/National Weather Service/NOAA/U.S. Department of Commerce, 2000, 2005). All physics parameterizations are the same, including Morrison double-moment microphysics (Morrison et al., 2005, 2009), RRTMG longwave radiation (Iacono et al., 2008), Goddard shortwave radiation (Chou & Suarez, 1999), the interactive Noah land surface model (LSM) (Niu et al., 2011; Yang et al., 2011), and MYNN level 3 boundary layer representation (Nakanishi & Niino, 2006, 2009). The WRF/Noah-LSM setup has been tested previously in the region over the United Arab Emeritus (UAE). Despite the hyper-arid environment, it was found to represent summertime heat fluxes quite accurately (Fonseca et al., 2020) or have a slight daytime and nighttime cold bias near the surface, which leads to an overestimation of heat fluxes (Chen et al., 2010; Nelli et al., 2020).

The GOCART module is used for online dust emissions. GOCART is a sectional model with five effective radius bins [0.5, 1.4, 2.4, 4.5, and 8.0 μm]. It predicts dust emissions with the following formula:

$$F_p = CSs_p U^2 \left(U - U_t\right) if\ U > U_t \quad (1)$$

where F_p is the dust flux from the surface [kg m^{-2} s^{-1}] for each of the radii bins (p) and is proportional to the 10-m wind speed (U) [m s^{-1}] and the threshold velocity of wind erosion (U_t) [m s^{-1}], which is a function of soil wetness. If the 10-m wind speed is less than the threshold velocity, no dust will loft from the surface. The terms (C,S,s_p) are time invariant scaling factors for total dust flux (C) [kg m^{-2} s^{-1}], soil erosion (S) [0 to 1], and the distribution of each size class within the soil (s_p) based on the silt and clay fraction of the soil type [0.1, 0.25, 0.25, 0.25, 0.25] that prescribes the size distribution. Both C and S are set to 1 for this study, and this setup differs from BvdH20 in that Ginoux et al. (2001) soil erodibility map is replaced with an idealized, horizontally homogeneous erodibility surface. Soil erodibility maps scale dust emissions from 0%–100% based on the likelihood the underlying soil type will loft dust. In our configuration, erodibility in each grid box is set to 100%, thus all locations are fully capable of lofting dust. Using idealized erodibility removes a degree of freedom in the analysis, for which there are multiple approaches and datasets with different representations (e.g., Ginoux et al., 2001; Prospero et al., 2002; Schepanski et al., 2007; Walker et al., 2009) of what is known to be a highly sensitive model parameter (Saleeby et al., 2019; Uno et al., 2006; BvdH20). This simplification overestimates the amount of dust-lofting regions, but removed the possibility of misleading interpretations due to the erodibility map.

The model was run from 00:00:00 to 18:00:00 UTC on August 2, 2016 with 5-min output using a one-way triple nest at 15:5:1.666 km (Figure S1 in Supporting Information S1). This grid setup is similar to BvdH20 with boundaries of the two coarser grids being the same, but run at 15:5 km instead of 45:15 or 15:3 km. The innermost nest was run with 1.666-km grid spacing and was centered around the specific storm in this case study and was not part of BvdH20. To better resolve cold pool processes near the surface, the vertical resolution was doubled from 50 stretched layers in BvdH20 to 100.

Dust radiation interactions in WRF-Chem (Barnard et al., 2010) are calculated online using Mie theory with a constant index of refraction across the SW bands of 1.550 + 0.003i and a spectrally varying refractive index in the LW (Table S2 in Supporting Information S1). WRF-Chem uses one index of refraction for dust, although evidence shows that minerology is location dependent and matters for representing the ratio of scattering to absorption, especially in the SW (Di Biagio et al., 2019, 2020; Journet et al., 2014; Li et al., 2021). The size distribution is also important when calculating aerosol radiative effects and recent literature demonstrates that models typically underestimate the coarse (radius > 10 μm) fraction of dust (Adebiyi & Kok, 2020; Huang et al., 2021). Since small dust particles are effective SW scatterers and large dust particles are effective LW absorbers (e.g., Hoshyaripour et al., 2019; Kok et al., 2017; Mahowald et al., 2014; Tegen & Lacis, 1996), the inclusion of more coarse dust could amplify the LW effects, while the daytime scattering effect may become less important.

Similar to BvdH20, the dust radiative effect was determined by holding all variables and model settings constant and running two simulations: one with active dust aerosol radiation (RAD) and one without

(NORAD). In the NORAD simulation, radiation is still active in the environment and impacts the meteorology and cloud microphysics, but excludes interactions with aerosol. The simulations were otherwise identical and Table S1 in Supporting Information S1 summarizes the model setup. To remove additional degrees of freedom, dust emissions in the GOCART module are only executed after the first downdrafts are identified at 10:00:00 UTC. Waiting for the cold pools to form eliminates uncertainties related to dust impacts on the storm structure, semi-direct effects, and initial formation of the density currents. It also excludes effects from diffuse airborne dust lingering in the atmosphere from other sources and ensures the analysis focuses solely on cold pool lofted dust. By prescribing dust emissions in this way, the only aerosol modifying the environment is dust lofted by the haboob itself.

2.3. Dust Feature Identification and Tracking

The convective system produces numerous cold pools that collide and interact throughout the simulation (Figures 2g–2i). These cold pools loft dust, but also contain areas of active precipitation that scavenge it (Figures 2a–2c, 2m–2o). To track the boundaries and mergers of these outflow elements and determine which portions of the outflow boundary contain dust requires an identification algorithm. Here, the offline post-processing Tracking and Object-Based Analysis of Clouds version 1.2 (TOBAC—Heikenfeld et al., 2019) framework was employed. TOBAC was originally developed to track convective updrafts and cloud volumes but is highly customizable and the code was modified in this study to identify and track dust within the density currents.

TOBAC works in three steps. First, it detects features in a 2D data field based on multiple threshold levels and attributes an area-weighted mean center to each. Including several thresholds rather than a single limit permits the algorithm to detect weak features while also assigning a more representative center to strong features. Surface dust concentration was selected as the 2D identification field, with thresholds of 1,200, 2,000, 3,000, and 4,000 $\mu g/m^3$, resulting in most of the dusty cold pool regions being identified while ignoring lower ambient dust concentrations outside of the haboob.

Several input variables were tested in the TOBAC framework for this experiment, including other more commonly tracked cold pool properties such as potential temperature (e.g., Drager & van den Heever, 2017). However, these properties do not specifically identify which regions of the cold pool contain dust. Feature identification using surface dust ensures that only the dusty regions of the cold pools are included in the analysis, which is inherently necessary for studying dust radiative effects and hence addressing our science goals. The decision to track on dust versus cold pool properties results in two competing yet incomplete outcomes: either non-dusty portions of the cold pool are included in an analysis meant to describe dust interactions, or dusty regions are analyzed as if they represent the entire density current when significant portions of the cold pool are pristine. To concentrate on dust effects, the latter option was selected with the caveat that it does not represent the entirety of the cold pool, or the interactions between dusty and pristine portions of the storm. A comparison of the dust features identified by TOBAC relative to the full outflow boundary is found in Figure 3.

Many tests were run with different dust thresholds to prevent the background concentrations from being identified, with the selected thresholds working well in the southern part of the domain, but some of the environmental air in the northern part of the domain was spuriously identified (Figure 3). To exclude any non-haboob features from the analysis, the northern and southern-most boundaries of the gust front were located and any TOBAC features identified outside those boundaries were discarded. Even though these portions of environmental air with high dust concentrations were removed from the TOBAC analysis, dust generated in the environment is still radiatively active and reduces the effect described here compared to a completely pristine environment. Nevertheless, for most of the domain during this simulation the environment contains orders of magnitude less dust than inside the haboob.

After locating dust features and their center points, the second step in TOBAC involves segmenting 3D volumes, in this case dust concentrations at the surface and aloft, with each identified feature using watershedding to connect and detach features that overlap, merge, or separate during their lifetime. Lastly, TOBAC tracks the 3D feature volumes and their centers in time through a finite difference method. In the end, TOBAC produces a database of independent 3D dust features within the haboob tracked in time

(Figures 3a–3c), allowing for composite and mean statistics to be performed on the database. A summary of the settings used to run TOBAC for this study can be found in Table S3 in Supporting Information S1.

2.4. Analysis Methods

2.4.1. Radiative Regimes

Because the dust radiative effect depends on the wavelength and intensity of radiation, the results are broken into three radiative regimes (Figure S3a in Supporting Information S1). This includes a daytime period with strong SW insolation at the surface, a transitional early evening period with low values of incoming SW, and a final LW-only period at night. The cutoff between day and evening is designated here as the time when the domain averaged incoming SW at the surface reaches half its initial value. To test if the daytime and/or evening results are sensitive to the exact temporal boundary, the threshold was moved 30 min backward and forward, but the sign of the responses did not change. Placement of the nighttime boundary is more straightforward and is set to when the domain averaged incoming SW reaches zero. It is possible for aged cold pool and haboob remnants to persist through the night and into the next morning (Heinold et al., 2013; Roberts & Knippertz, 2014), but examining such effects was outside the scope of this study. Dust radiation interactions in a haboob could also have impacts on longer timescales than those presented here, but those feedbacks are left for further study.

2.4.2. Focus on Surface Values

Convective cold pools are limited in their vertical extent and the conditions within a cold pool relevant to the lifting of dust are inherently near-surface. As such, the analysis will not examine the full vertical thermodynamic or dust profile. Inspecting mean vertical profiles of dust and aerosol heating rates (Figure S2 in Supporting Information S1), the maximum dust concentrations, and consequently the strongest radiative feedbacks, are contained within a shallow layer near the surface below 1.0–1.5-km AGL. Cold pool temperature, dust, and direct effects decrease exponentially from the surface (BvdH20), although these can be important from an integrated standpoint. As such, outside of integrated dust values, the analysis in Section 3 focuses on surface or lowest model level quantities where appropriate.

2.4.3. Normalization and Detection Differences

Despite running TOBAC identically on both the RAD and NORAD simulations to produce two databases of tracked cold pool features, dissimilarities in the detection between the two simulations are apparent and are expected. The dust radiative effect alters the environment, which leads to differences in the physical processes and dust concentrations. As dust concentrations change, they affect the area of the domain that meets the feature detection threshold. TOBAC correctly identifies these differences and tracks the unique cold pool movements, and the merging of features in each simulation. Nonetheless, the distinct detections in each case prevents a one-to-one/feature-to-feature comparison due to the specific feature number and area identified in the RAD and NORAD case (Figure S3b in Supporting Information S1). The most significant difference in the area of identified features occurs around 15:00:00 UTC, with more dust area in the RAD simulation, but is otherwise close between the two simulations. Because of the detection differences, all results are presented from a composite framework via histograms normalized by the number of identified points in each time block.

In general, the difference in the number of points does not change the results when normalized, except for surface dust concentrations and integrated dust at the latter portion of the evening and full nighttime periods. Not accounting for feature area, there is more dust in the RAD case in all time periods (Figures S3c and S3e in Supporting Information S1). However, when the feature area is included, the sign reverses in the transitional case and at night, with the NORAD case producing higher dust concentrations (Figures S3d and S3f in Supporting Information S1) for roughly 1 hr between 15 and 16 UTC before returning to the original trend. Therefore, the results for evening and nighttime surface dust concentration and integrated dust are ambiguous for the transition period. All variables were tested for this dubious inversion from the normalization process, but it presented only in these two variables. We hypothesize that the dust-on-dust feedback is inconclusive because dust concentration was used as the tracking variable, which then influences the use of dust as an analysis variable. It is possible that this inconclusive result would appear in whichever variable

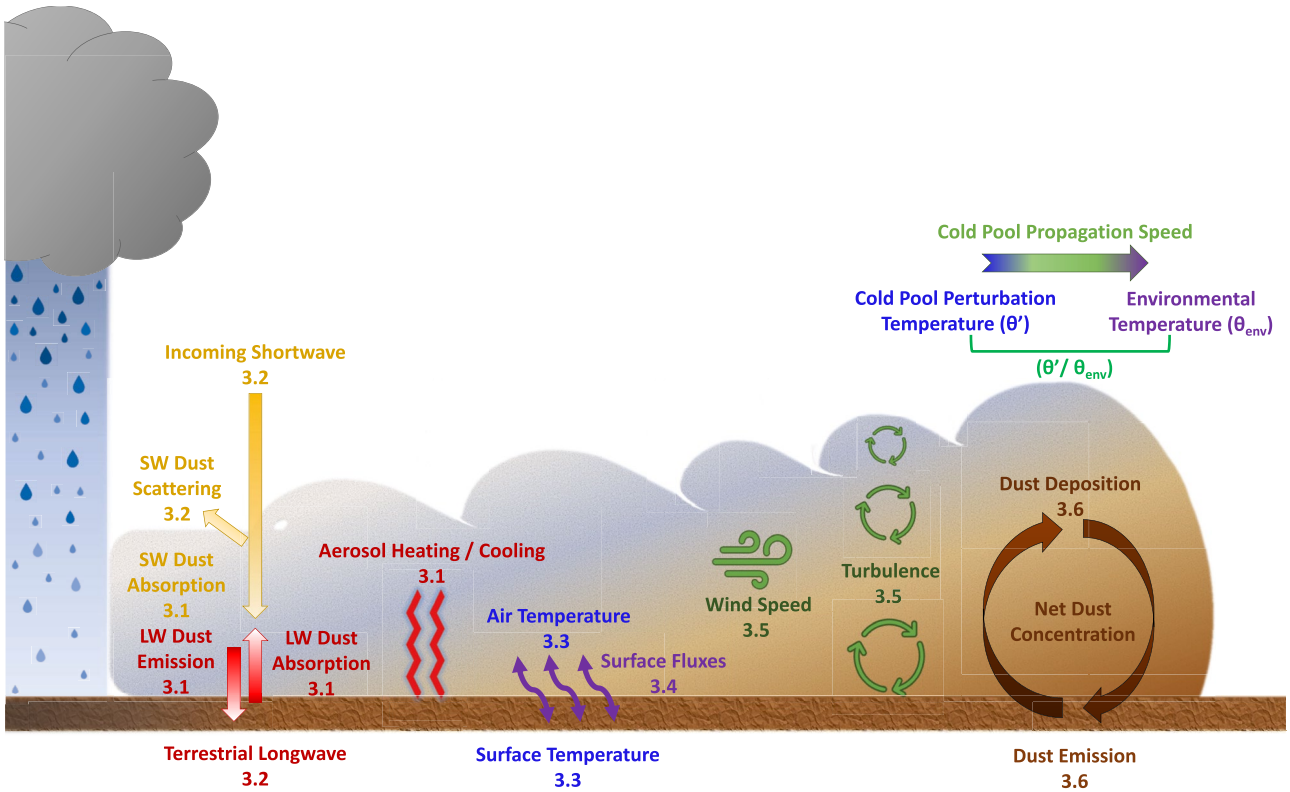

Figure 4. The "dust direct effect cascade:" a conceptual schematic representing the physical processes impacted by the dust radiative effect in a density current. The numbers refer to the section discussing each mechanism.

was selected as the cold pool tracking field (e.g., temperature and wind) if there is a large enough difference in the number or area of tracked objects between the simulations. As such, dust emission and settling flux present a more realistic picture of the dust-on-dust feedbacks than concentration.

All TOBAC-identified data points from the RAD and NORAD simulations are collected into three bins based on the day, transition, and night classification and represented as relative, or normalized, probability histograms in Figures 5–9. The histogram bars are the number of haboob grid points that match the bin values divided by the total number of grid points identified by TOBAC for that time period. The sum of the bar heights will equal 1. This allows us to compare the RAD and NORAD cases despite TOBAC identifying a different total number of grid points for each.

3. Results

When dust aerosol is lofted by cold pools, it interacts with solar and terrestrial radiation. It will scatter and absorb, leading to changes in the properties of several variables, including the haboob's dynamics. The catalyst of the dust radiative feedback mechanism is the aerosol heating rate of the atmosphere (Section 3.1). This heating imbalance alters SW and LW radiation at the surface (Section 3.2) and goes on to modify surface temperatures (Section 3.3). This difference in temperature affects surface heat fluxes (Section 3.4), turbulence, winds, cold pool propagation speed, and stability (Section 3.5), which directly alter the amount of dust lofted and deposited inside the cold pools (Section 3.6). This chain reaction of feedbacks culminates in the dust concentration of the haboob, which is the net inequality between emission and settling rates. The effect dust has on these physical mechanisms depends on the wavelength of radiation, dust concentrations, and environmental conditions. Each part of this direct dust radiative mechanism is split into day/evening/night. A conceptual schematic of the processes in a density current that are directly or indirectly altered by the dust direct effect cascade are found in Figure 4.

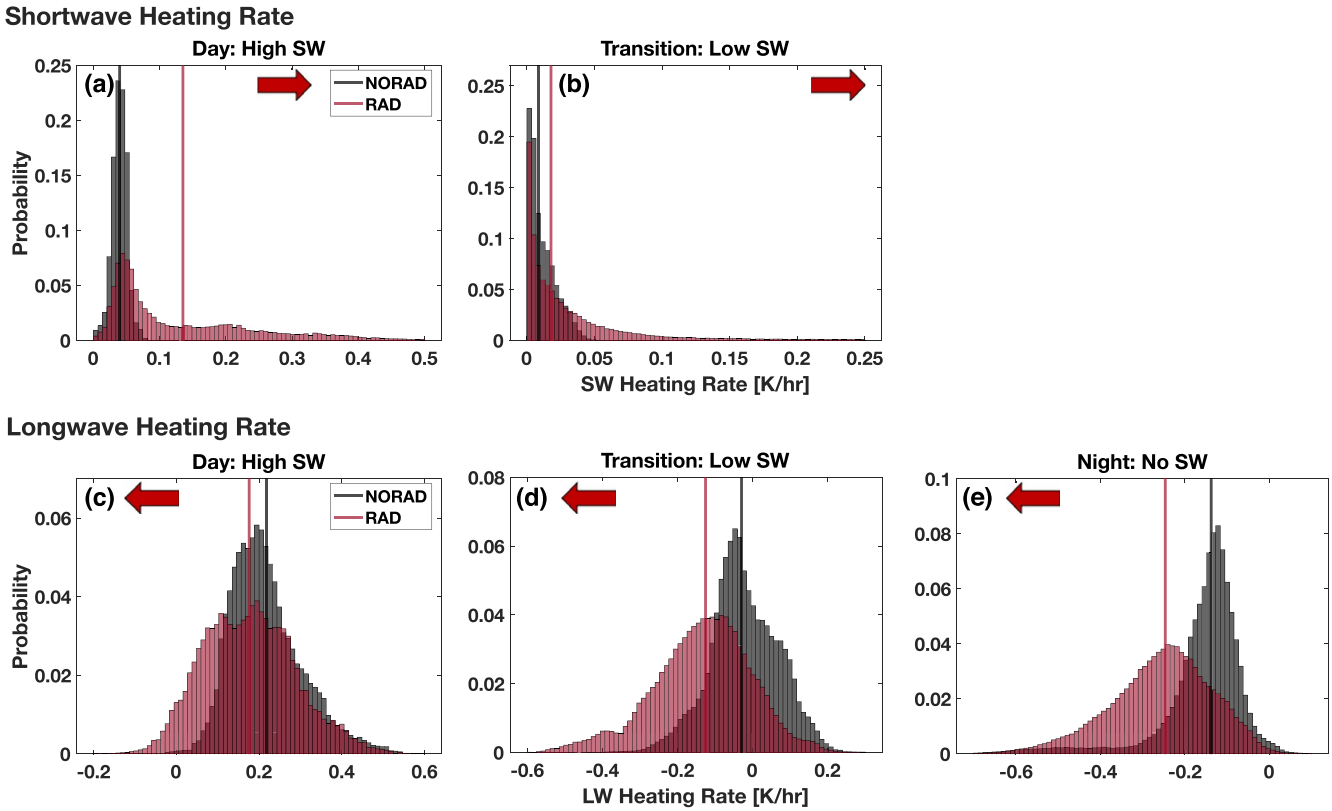

Figure 5. Normalized probability histograms of the shortwave (a) and (b) and longwave (c)–(e) heating rates for the three analysis time periods for the Tracking and Object-Based Analysis of Clouds-tracked dust features in the NORAD (gray) and RAD (dark red) simulations. The vertical lines represent the median of each distribution. Arrows pointing toward the left indicates a shift in the distribution to lower values (decrease) when dust radiation is included, with the opposite arrow orientation indicating a shift toward higher values (increase) from including aerosol radiative interactions.

3.1. Aerosol Heating Rates

During the day, dust in the cold pools scatters SW radiation, preventing it from reaching the surface. Simultaneously, dust absorbs some of the incoming SW and heats dusty layers aloft. The absorption of SW is represented by positive perturbations to atmospheric heating rates and is evident by the increase in the SW heating rate in the RAD simulation of the TOBAC-tracked cold pool dust (Figure 5a). This increase reaches a maximum of 0.5 K hr^{-1} in the density currents, although the median of the distribution is closer to 0.1 K hr^{-1}. The maximum and median heating rates constrain the length of time a haboob must exist for the dust effects to be felt by the local atmosphere. Weak effects must either exist in greater number or for a longer period of time to have an effect. Additionally, dust absorbs and emits in the LW, which corresponds to a negative heating (cooling) rate as the atmosphere radiates more energy to achieve balance. In the daytime, the RAD simulation has lower values (Figure 5c), or more LW absorption and emission than the NORAD simulation. The same results are evident in the evening transition, with higher SW heating rates (Figure 5b) and more LW emission (Figure 5d) in the RAD case, while the relative importance of each effect reverses; in the daytime, the SW aerosol heating rate is higher, while in the evening the LW component dominates.

At night the SW is zero, but the LW effect is at its strongest (Figure 5e), with the absolute value of the median nighttime LW heating rate being higher than the SW rate during the day. While SW effects may have been found to be relatively more important for large-scale dust sources (Saleeby et al., 2019; BvdH20), the LW effect appears to be just as, if not more important than the SW effects on the mesoscale in the gust front case.

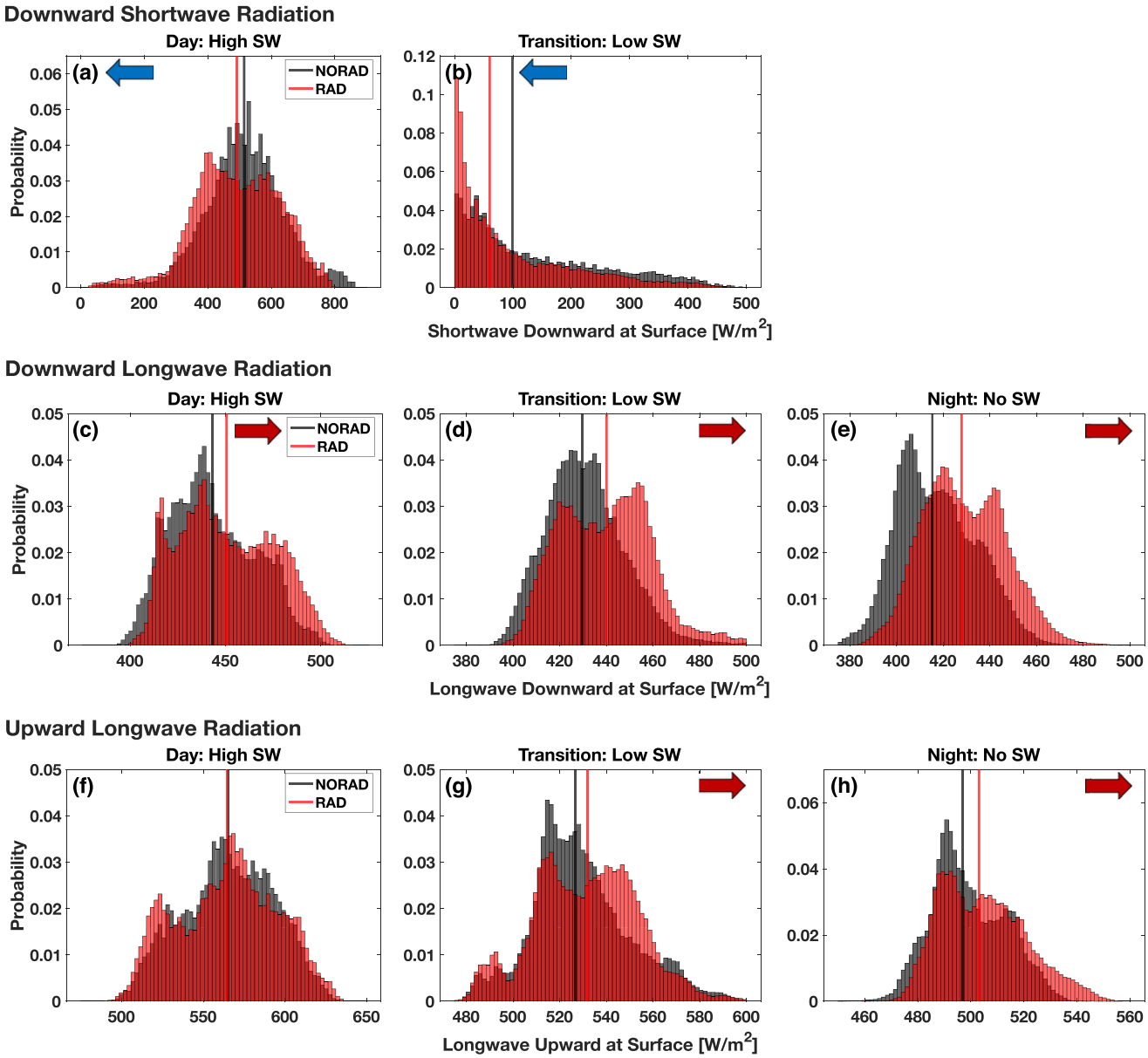

Figure 6. Same as Figure 5, but for surface (a)–(c) downward SW, (d)–(f) downward LW, and (f)–(h) upward LW radiation.

3.2. Surface Shortwave and Longwave Radiation

The scattering and absorbing of SW radiation in the dusty cold pool leads to less SW being transmitted to the surface in both the daytime and evening periods of the RAD case (Figures 6a and 6b). Additionally, there is a shift toward more LW directed downward to surface in all three time periods (Figures 6c–6e) due to the SW/LW absorption and emission, which radiates isotropically and results in some portion of radiation being directed downward. Due to the competition between the reduction in SW and the increase of LW downward at the surface during the day, terrestrial radiative fluxes between the surface and the atmosphere change in both directions and do not present a clear shift (Figure 6f), which has been noted in other studies as well (Mallet et al., 2009; Marsham et al., 2016; Miller et al., 2004; Saleeby et al., 2019). However, in the evening as the SW effect becomes less important, the LW dust effect again begins to dominate and increases in the RAD case (Figure 6g). This same shift in LW is also apparent at night after the SW component no longer contributes to the radiation balance (Figure 6h).

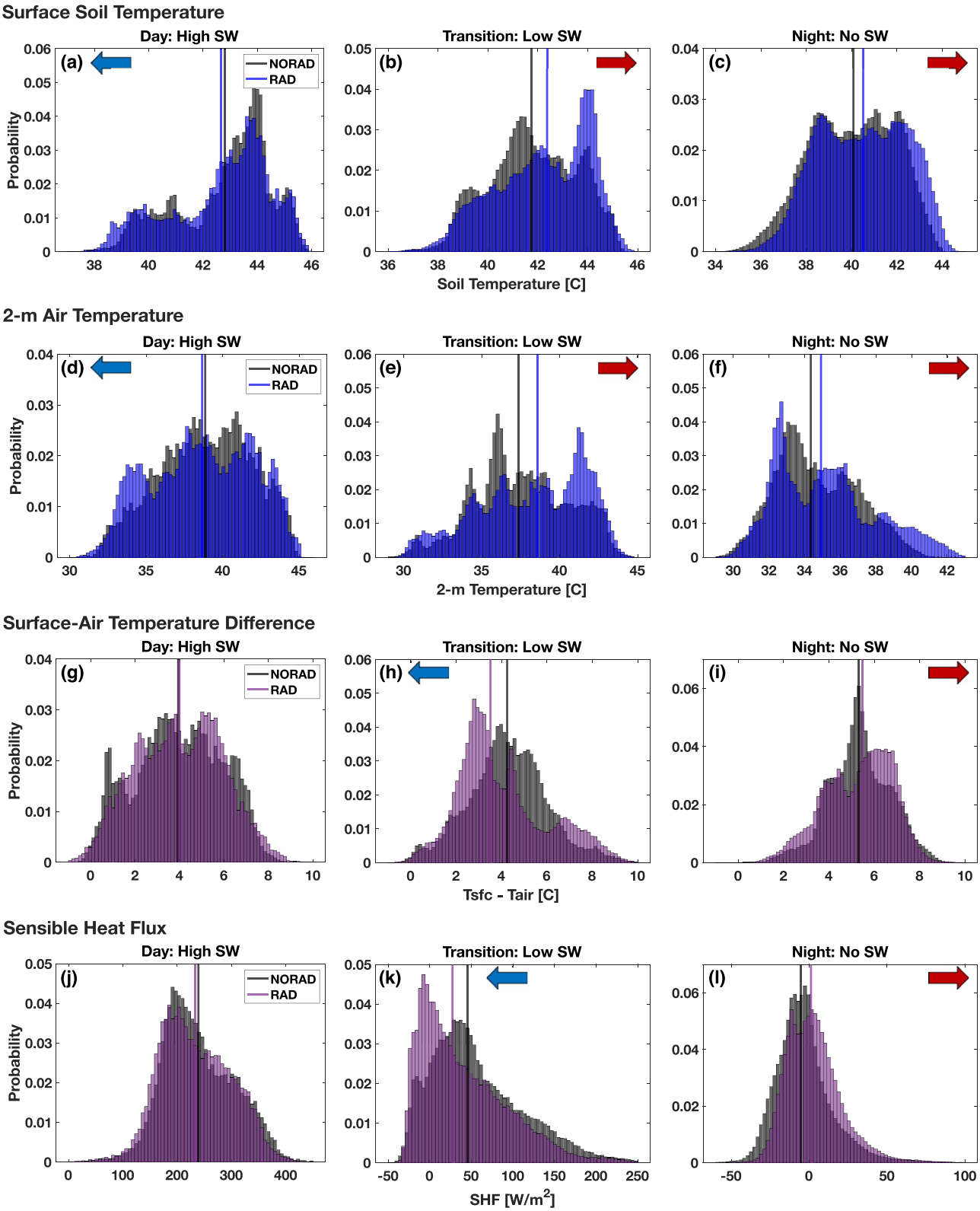

Figure 7. Same as Figure 5, but for (a)–(c) surface soil temperature, (d)–(f) 2-m air temperature, (g)–(i) surface-air temperature difference, and (j)–(l) sensible heat flux.

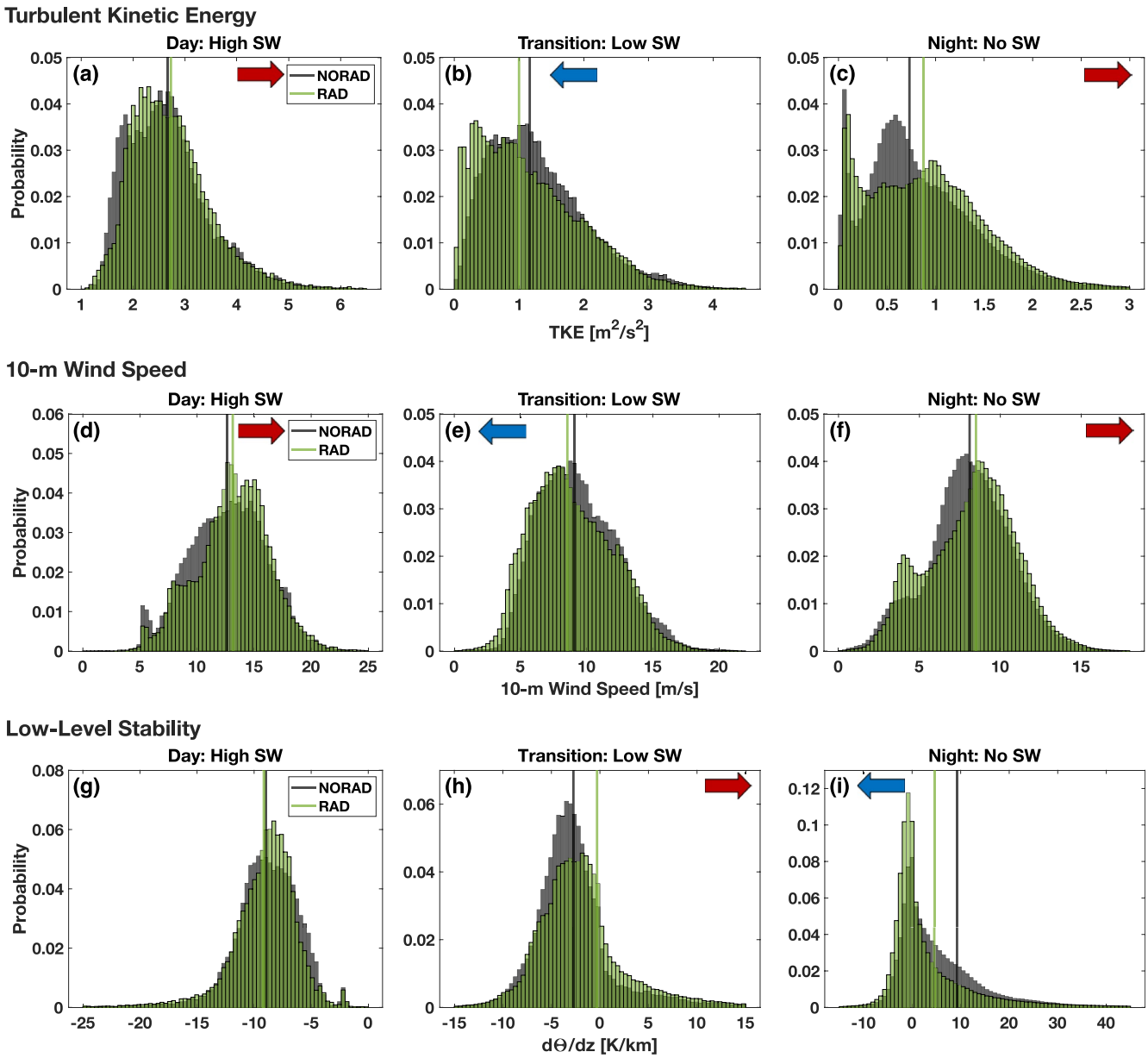

Figure 8. Same as Figure 5, but for surface (a)–(c) turbulent kinetic energy, (d)–(f) 10-m windspeed, and (g)–(i) lowest-level stability.

3.3. Surface and Near-Surface Air Temperature

Daytime SW scattering by haboob dust in the RAD case exceeds LW absorption/emission when incoming SW is high, leading to lower surface temperatures being more likely (Figure 7a). Because the surface temperatures are lower, the air above the surface is also cooler when dust radiative effects are present (Figure 7d). Density currents are driven by the temperature (and hence density) difference between cold pool air and the environmental air around it. The theoretical cold pool strength is often calculated with the following equation (Benjamin, 1968; Rotunno et al., 1988):

$$V^2 = 2\int_0^H -g\frac{\theta'}{\theta_{env}}dz \quad (2)$$

where V is the theoretical cold pool speed (m s^{-1}), or intensity, H is the cold pool depth (m), g is gravitational acceleration (m s^{-2}), dz is the model vertical grid spacing (m), θ' is the cold pool perturbation potential

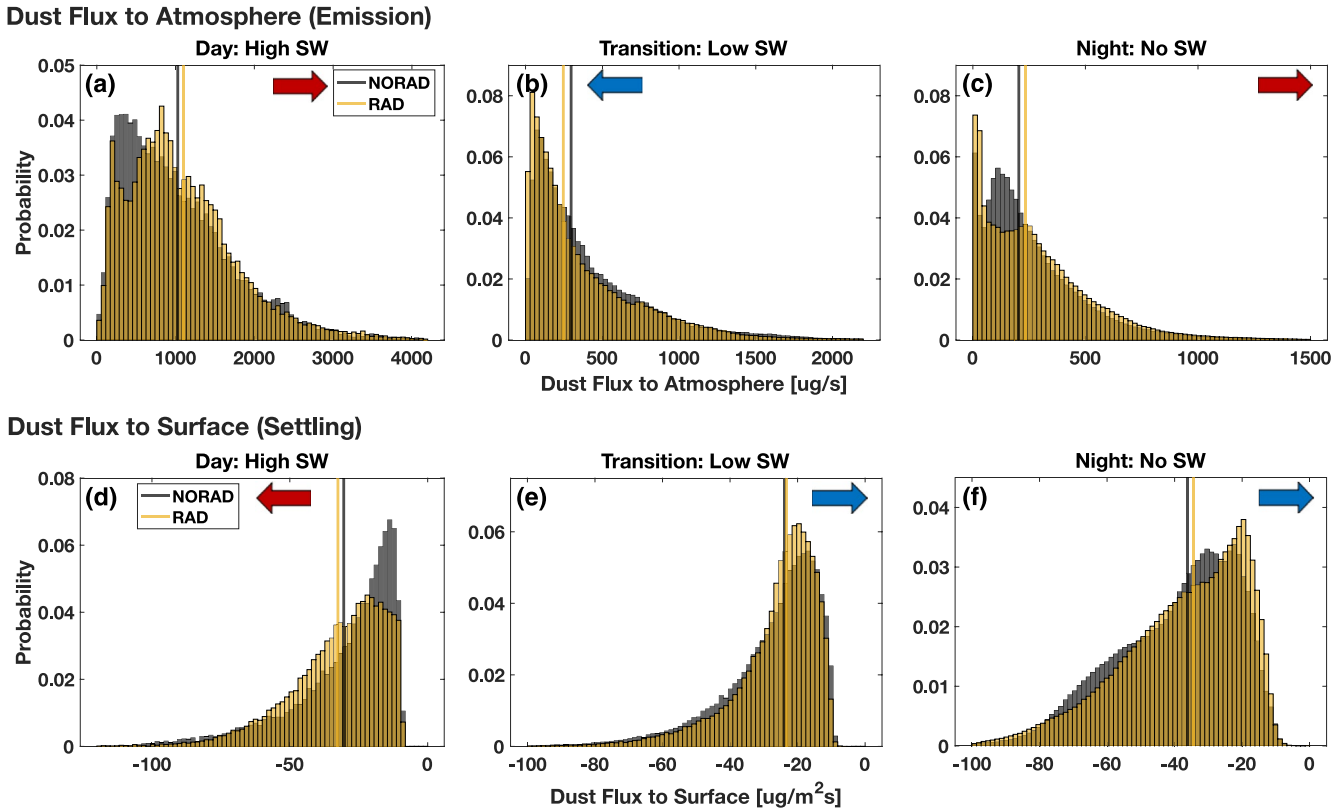

Figure 9. Same as Figure 5, but for surface (a)–(c) dust flux to atmosphere, and (d)–(f) dust flux to the surface (dry deposition + gravitational settling). Note that because dust settling flux is designated as a negative value the arrows in panels (d)–(f) are opposite.

temperature (K) relative to the mean air outside the density current, θ_{env} (K), with θ' calculated as a simple difference between the environmental air and the cold pool air ($\theta' = \theta_{env} - \theta_{cold\ pool}$). From Equation 2, a larger gradient between cold pool air and environmental air ($\frac{\theta'}{\theta_{\mathrm{env}}}$) leads to a more intense, faster traveling cold pool. With dust radiation, scattering leads to colder temperatures in the cold pool compared to the less-dusty ambient environment. This implies that the density current is stronger, or more intense, when dust is present during the day, and these cold pools will spread away from their parent storms more rapidly. This result echoes the findings of Chen et al. (1995), who found that scattering inside a dusty cold front led to a colder surface temperature and a stronger temperature gradient between the front and the pristine environment.

Nevertheless, the trend reverses in the evening and nighttime when the LW effect dominates. With LW absorption and emission, surface temperatures and air temperatures near the surface do not cool as rapidly as they normally would in a clear-sky scenario. Thus, nocturnal cold pools are warmer when laden with dust (Figures 7b, 7c, 7e, and 7f) than a pristine cold pool would be. Because the temperature differential between the cold pool and the large-scale environment is reduced, from Equation 2, the haboob should be weaker, or less intense at night, and as a result propagate more slowly in relation to a pristine cold pool. Interestingly, the nocturnal behavior of haboobs is more complicated than the relationship in Equation 2 can describe and is discussed in more detail in the following sections.

3.4. Surface Heat Flux

As the dust radiative effect modifies surface and near-surface air temperatures, SHFs also change. SHFs are often represented by the following equation:

$$\mathrm{SHF} = \mathrm{C_d C_p \rho_{air} U}\left(\mathrm{T_{sfc}} - \mathrm{T_{air}}\right) \quad (3)$$

where C_d is an aerodynamic bulk transfer coefficient, C_p is the heat capacity of dry air at constant pressure (J kg^{-1} K^{-1}), ρ_{air} is the density of air (kg m^{-3}), U is the near-surface wind speed (m s^{-1}), and T_{sfc} and T_{air} are the temperature of the surface and the near-surface air (K^{-1}) respectively.

The daytime haboob is colder and therefore denser when accounting for dust radiative effects, which leads to higher windspeeds (Section 3.5). Because of SW scattering, the distribution for surface temperature and the near-surface air both shift toward lower temperatures (Figures 7a and 7d). However, there is a reduction in the magnitude of the T_{sfc}–T_{air} difference (Figure 7g) between the RAD and NORAD simulations. As a consequence, the positive and negative contributions cancel, leading to little change in the daytime SHFs. This outcome is inconsistent with other studies that show a reduction in SHF during the day due to suppressed surface temperatures from the dust scattering effect (Alamirew et al., 2018; Fan et al., 2008; Heinold et al., 2007; Jiang & Feingold, 2006; Mallet et al., 2009; Miller et al., 2004; Pérez et al., 2006; Saleeby et al., 2019). This discrepancy may stem from previous studies focusing on synoptic or climate-scale dust cases, whereas this study specifically investigates mesoscale cold pools. In a cold pool the substantial temperature shift that increases SHFs is absent in large-scale circulations in the Arabian Peninsula, but may be similar to features such as cold fronts. Here, the land surface must respond concurrently to the cold air perturbation from the density current and dust aerosol effects. The abrupt drop in T_{air} as the density current passes produces a strong positive SHF response, or fluxes directed from the surface to the air, that dominate over the SHF decrease from the daytime SW feedback.

In the day, the SW effect first leads to a cooler surface, which in turn prevents the air above it from warming through longwave heating. Conversely, in the evening and nighttime, the LW aerosol effect traps heat aloft first, which then warms the surface. In the transitional evening case, the surface begins to cool as the incoming solar radiation vanishes. However, terrestrial radiation is trapped by dust, which radiates downward and prevents the surface from cooling as rapidly as it would in a pristine aerosol case. Both T_{air} and T_{sfc} increase because of this LW effect, but T_{air} increases faster than T_{sfc}, leading to a reduction in the surface-air temperature difference (Figure 7h). Coupled with the warmer, weaker and less dense cold pool in the RAD case, SHFs are reduced during the evening and are more likely to be negative, or directed from the air to the ground, than in the NORAD simulations.

After the sun has set, both the surface and the near-surface air are warmer due to the dust LW effect. However, there is now a larger surface-air difference in the RAD nighttime case as the terrestrial radiation is trapped and the layers above it cool as they flux toward and away from the surface. The relatively warmer dusty cold pools are less dense, but SHFs increase due to higher windspeeds at night (Section 3.5).

3.5. Turbulence, Wind, and Low-Level Stability

Changes to the temperature of the density currents relative to the environment drive changes to their intensity and their propagation speeds. In the daytime, the simulated cold pools are colder in the RAD experiment due to the dust scattering effect, which leads to stronger in-cold pool windspeeds (Figure 8d), and thus higher values of TKE (Figure 8a). This results in daytime cold pools being more intense and moving faster due to the impacts of dust radiative effects.

In the transitional period, LW dust absorption and emission leads to a warmer density current with lower windspeeds (Figure 8e) and suppressed TKE (Figure 8b) in the RAD simulation. The presence of dust within the cold pool also enhances low-level stability (Figure 8h) due to the air aloft being warmer than the cooling surface from the LW effect (Section 3.4). Therefore, the evening portion produces cold pools that are relatively weaker and move slower in the radiation case.

At night, dust radiative effects are less straightforward: the cold pool is warmer due to the LW effect (Figure 7c), but there are higher windspeeds (Figure 8f) and enhanced turbulence (Figure 8c) inside the haboob. This result contradicts the theory that a reduced temperature gradient between a cold pool and its environment should lead to reduced windspeed and intensity (Equation 2). However, when dust radiation is included, the LW effect prevents the surface from cooling as strongly as it would under clear conditions that typically stabilize the nocturnal boundary layer. The LW warming leads to a less stable surface layer (Figure 8i) that retains some of the buoyant contribution to TKE and windspeed that were already depleted in the pristine case.

While the dusty portions of the cold pool are less stable, the pristine desert environment around the haboob cools rapidly, leading to a strong inversion and statically stable conditions. It has been shown that the stability of the environment into which a density current propagates affects its height and propagation speed (Liu & Moncrieff, 2000; Seigel & van den Heever, 2012b). Seigel and van den Heever (2012b) tested the effect of the static stability of a thin surface stable layer on cold pools, similar to a nocturnal desert inversion. They found that a more statically stratified environment surrounding a cold pool leads to a shallower and faster moving density current due to an increased horizontal pressure gradient behind the gust front. In essence, the cold pool must accelerate as it is forced underneath a surface inversion. We hypothesize that the warmer, dusty cold pool exhibits higher values of TKE from the enhanced and more positive SHFs, which leads to more vertical development. Conversely, the colder, pristine cold pool is more stable and less turbulent due to suppressed and more negative heat fluxes, leading to a shallower, denser air mass. Both cold pools are forced under the same inversion, but the warmer, loftier, dusty cold pool is squeezed more and must accelerate faster. There are undoubtedly competing results here: the warmer cold pool should move slower via the reduced temperature gradient between it and the environment (Equation 2), but the static stability and inversion height between the two also matter for cold pool propagation in the nocturnal case as in Seigel and van den Heever (2012b). This hypothesis requires further testing and we speculate that this effect would be highly sensitive to the depth and strength of the cold pool and the nocturnal inversion layer in different environments.

3.6. Dust Emission and Settling Rates

Modifications to wind and stability near the surface will feedback on dust emissions and settling rates. Dust flux to the atmosphere is primarily a function of wind speed, but it can be modified by soil erodibility and soil wetness. Here, soil erodibility is set to a constant value by design and the parent storm is not affected by dust radiation (i.e., no significant alteration to precipitation or soil moisture), thus changes in windspeed drive the observed changes in dust emission rates. Higher windspeeds in the day enhance dust emissions, lower windspeeds in the evening suppress emissions, and stronger winds at night support higher emissions (Figures 9a–9c).

Dust flux from the air to the surface, or dust removal, depends on the combination of turbulent transfer toward the surface, or dry deposition, and gravitational settling, the latter of which is inversely proportional to the viscosity of air and therefore inversely proportional to temperature. In the GOCART model and for this case study, gravitational settling is the dominant dry removal mechanism. Here we have added these two processes together into a combined dry dust flux to the surface. In the day, lower temperatures and higher TKE in the RAD simulations leads to more dust being removed from the atmosphere (Figure 9d). In the evening, warmer temperatures and suppressed TKE both support lower dust fluxes to the surface (Figure 9e), while at night warmer temperatures compete with enhanced TKE, but ultimately dust fluxes to the surface are reduced (Figure 9f).

Dust concentrations at any given point are a balance between emissions, transport, and deposition, and the self-imposed feedback of dust radiation on dust concentrations is the culmination of a cascade of processes altered by the dust radiative effect, as represented by the schematic in Figure 4. From Figure S3 in Supporting Information S1, domain-wide there are higher dust concentrations in the RAD case throughout the entire simulation period, supported by the fact that more cells are identified over the dust threshold of 1,200 [ug m^{-3}] in the RAD simulation. Nevertheless, when normalized by detected area, the distributions are inconclusive or may present an opposite result (Section 2.4) and more work is needed to understand the dust-on-dust feedback mechanism.

4. Discussion and Conclusions

This study examines the impacts of dust-radiation interactions on cold pool processes and associated feedbacks. To quantify these effects, an Arabian Peninsula convective outflow dust event was simulated using WRF-Chem with and without dust radiation interactions. The TOBAC framework was used to track and identify the dusty regions of the numerous cold pool boundaries and create histograms of cold pool properties for both simulations as a function of three distinct radiative regimes based on insolation: daytime (high SW), evening transition (low SW), and night (LW only). A summary of direct dust feedbacks on cold pool

Table 1
Summary of the Dust Radiative Responses in the Haboob

Parameter	Day (High SW)	Transition (Low SW)	Night (No SW)
SW heating rate	Increase	Increase	None
LW heating rate	Increase	Increase	Increase
Surface SW downward	Decrease	Decrease	None
Surface LW downward	Increase	Increase	Increase
Surface LW upward	Null	Increase	Increase
2-m air temperature	Decrease	Increase	Increase
Soil temperature	Decrease	Increase	Increase
$T_{sfc}-T_{air}$	Decrease	Decrease	Increase
Sensible heat flux	Null	Decrease	Increase
Turbulent kinetic energy	Increase	Decrease	Increase
10-m windspeed	Increase	Decrease	Increase
Low-level stability	Null	Increase	Decrease
Dust emission rate	Increase	Decrease	Increase
Dust settling rate	Increase	Decrease	Decrease

processes can be found in the schematic in Figure 4, and the impact on each mechanism can be found in Table 1.

During the day, dust scatters SW radiation, reduces insolation, cools the surface and air above it, and increases the temperature gradient between the cold pools and their parent environment. This leads to stronger density currents with higher windspeeds, enhanced turbulence, and increased dust emissions and concentrations. Unlike the synoptic-scale dust events previously examined in the literature, SHFs during the day are not reduced by the SW scattering effect because the strong positive SHF response due to the cold air perturbation from the density current and associated enhanced windspeeds dominate compared to the dust radiation signal. In the evening transition between day and night, dust LW absorption aloft and emission toward the surface becomes more important than the diminishing SW component. This leads to a warmer surface and cold pools with a reduced temperature gradient between cold pool air and the environment, resulting in weaker density currents with suppressed TKE, windspeeds, dust lofting, and SHFs. At night, the LW warming persists, but the trapped LW leads to a less stable nocturnal cold pool than if radiative cooling had occurred in a pristine environment. Therefore, the outflow boundary is warmer, but not necessarily weaker according to Equation 2 because it contains stronger windspeeds, enhanced TKE and SHFs, and higher dust emissions, which we hypothesize is due to the less stable haboob air moving into the pristine and statically stable nocturnal boundary layer.

These results need to be expanded to different storms and environments and may be highly sensitive to timing, insolation, ambient dust concentrations and dust mineralogy, surface properties, and model parameters such as the refractive index, spherical dust assumptions, and the size partitioning of dust mass. The effect that dust radiation has on nocturnal haboob remnants as they age through the night and into the next morning and what impact this has on the environment also warrants future work. More case studies and understanding the higher order effects such as dusty/pristine collisions and understanding dust-on-dust feedbacks will require further study.

Nevertheless, the results here can be applied to the forecasting of haboobs. To first order, dust radiative feedbacks will lead to a colder, dustier, faster moving cold pool in the day. In the early evening, haboobs can be expected to be warmer, slower, and will loft less dust as they travel, whereas at night, a haboob will be warmer, but gustier in the more stable nocturnal surface layer. These identified feedbacks of dust radiation on cold pool properties are a first step toward understanding dust radiative effects in mesoscale dust events, such as convective outflow boundaries, and the effect that different radiative regimes has on this phenomenon.

Conflict of Interest

The authors declare no conflicts of interest relevant to this study.

Data Availability Statement

Namelists required to reproduce the WRF-Chem simulations, commented Python code and WRF input files used to run the TOBAC postprocessing tool, and links to all publically available source codes and datasets used in this study can be found in the following data repository: http://dx.doi.org/10.25675/10217/233939.

Acknowledgments
This work was funded by an Office of Naval Research–Multidisciplinary University Research Initiative (ONR-MURI) grant (N00014-16-1-2040).

References

Adebiyi, A., & Kok, J. F. (2020). Climate models miss most of the coarse dust in the atmosphere. *Science Advances*, *6*, eaaz9507. https://doi.org/10.1126/sciadv.aaz9507

Alamirew, N. K., Todd, M. C., Ryder, C. L., Marsham, J. H., & Wang, Y. (2018). The early summertime Saharan heat low: Sensitivity of the radiation budget and atmospheric heating to water vapour and dust aerosol. *Atmospheric Chemistry and Physics*, *18*, 1241–1262. https://doi.org/10.5194/acp-18-1241-2018

Alizadeh Choobari, O., Zawar-Reza, P., & Sturman, A. (2013). Low level jet intensification by mineral dust aerosols. *Annales Geophysicae*, *31*, 625–632. https://doi.org/10.5194/angeo-31-625-2013

Baddock, M. C., Strong, C. L., Murray, P. S., & McTainsh, G. H. (2013). Aeolian dust as a transport hazard. *Atmospheric Environment*, *71*, 7–14. https://doi.org/10.1016/j.atmosenv.2013.01.042

Banks, J. R., Brindley, H. E., Hobby, M., & Marsham, J. H. (2014). The daytime cycle in dust aerosol direct radiative effects observed in the central Sahara during the Fennec campaign in June 2011. *Journal of Geophysical Research: Atmosphere*, *119*, 13861–13. https://doi.org/10.1002/2014JD022077

Barbaro, E., Vilà-Guerau de Arellano, J., Krol, M. C., & Holtslag, A. A. M. (2013). Impacts of aerosol shortwave radiation absorption on the dynamics of an idealized convective atmospheric boundary layer. *Boundary-Layer Meteorology*, *148*, 31–49. https://doi.org/10.1007/s10546-013-9800-7

Barnard, J., Fast, J., Paredes-Miranda, G., Arnott, W., & Laskin, A. (2010). Technical note: Evaluation of the WRF-Chem "aerosol chemical to aerosol optical properties" module using data from the MILAGRO campaign. *Atmospheric Chemistry and Physics*, *10*, 7325–7340. https://doi.org/10.5194/acp-10-7325-2010

Benjamin, T. B. (1968). Gravity currents and related phenomena. *Journal of Fluid Mechanics*, *31*, 209–248. https://doi.org/10.1017/S0022112068000133

Bryan, G. H., & Rotunno, R. (2014). Gravity currents in confined channels with environmental shear. *Journal of the Atmospheric Sciences*, *71*, 1121–1142. https://doi.org/10.1175/JAS-D-13-0157.1

Bukowski, J., & van den Heever, S. C. (2020). Convective distribution of dust over the Arabian Peninsula: The impact of model resolution. *Atmospheric Chemistry and Physics*, *20*, 2967–2986. https://doi.org/10.5194/acp-20-2967-2020

Carlson, T. N., & Benjamin, S. G. (1980). Radiative heating rates for Saharan dust. *Journal of the Atmospheric Sciences*, *37*(1), 193–213. https://doi.org/10.1175/1520-0469(1980)037<0193:rhrfsd>2.0.co;2

Chen, W., & Fryrear, D. W. (2002). Sedimentary characteristics of a haboob dust storm. *Atmospheric Research*, *61*(1), 75–85. https://doi.org/10.1016/S0169-8095(01)00092-8

Chen, D., Liu, Z., Davis, C., & Gu, Y. (2017). Dust radiative effects on atmospheric thermodynamics and tropical cyclogenesis over the Atlantic Ocean using WRF-Chem coupled with an AOD data assimilation system. *Atmospheric Chemistry and Physics*, *17*, 7917–7939. https://doi.org/10.5194/acp-17-7917-2017

Chen, S.-J., Kuo, Y.-H., Ming, W., & Ying, H. (1995). The effect of dust radiative heating on low-level frontogenesis. *Journal of the Atmospheric Sciences*, *52*, 1414–1420. https://doi.org/10.1175/1520-0469(1995)052<1414:TEODRH>2.0.CO;2

Chen, Y., Yang, K., Zhou, D., Qin, J., and Guo, X. (2010). Improving the Noah land surface model in arid regions with an appropriate parameterization of the thermal roughness length. *Journal of Hydrometeorology*, *11*(4), 995–1006. https://doi.org/10.1175/2010JHM1185.1

Chou, M.-D., & Suarez, M. J. (1999). Technical report series on global modeling and data assimilation: A thermal infrared radiation parameterization for atmospheric studies revised May 2003. *National Aeronautics and Space Administration Technical Memorandum*, *15*, 40.

Cowie, S. M., Marsham, J. H., & Knippertz, P. (2015). The importance of rare, high-wind events for dust uplift in northern Africa. *Geophysical Research Letters*, *42*, 8208–8215. https://doi.org/10.1002/2015GL065819

Di Biagio, C., Formenti, P., Balkanski, Y., Caponi, L., Cazaunau, M., Pangui, E., et al. (2019). Complex refractive indices and single-scattering albedo of global dust aerosols in the shortwave spectrum and relationship to size and iron content. *Atmospheric Chemistry and Physics*, *19*, 15503–15531. https://doi.org/10.5194/acp-19-15503-2019

Di Biagio, C., Balkanski, Y., Albani, S., Boucher, O., & Formenti, P. (2020). Direct radiative effect by mineral dust aerosols constrained by new microphysical and spectral optical data. *Geophysical Research Letters*, *47*, e2019GL086186. https://doi.org/10.1029/2019GL086186

Drager, A. J., & van den Heever, S. C. (2017). Characterizing convective cold pools. *Journal of Advances in Modeling Earth Systems*, *9*, 1091–1115. https://doi.org/10.1002/2016MS000788

Drager, A. J., Grant, L. D., & van den Heever, S. C. (2020). Cold pool responses to changes in soil moisture. *Journal of Advances in Modeling Earth Systems*, *12*, e2019MS001922. https://doi.org/10.1029/2019MS001922

Fan, J., Zhang, R., Tao, W.-K., & Mohr, K. I. (2008). Effects of aerosol optical properties on deep convective clouds and radiative forcing. *Journal of Geophysical Research*, *113*, D08209. https://doi.org/10.1029/2007JD009257

Fast, J. D., Berg, L. K., Feng, Z., Mei, F., Newsom, R., Sakaguchi, K., & Xiao, H. (2019). The impact of variable land-atmosphere coupling on convective cloud populations observed during the 2016 HI-SCALE field campaign. *Journal of Advances in Modeling Earth Systems*, *11*, 2629–2654. https://doi.org/10.1029/2019MS001727

Fast, J. D., Gustafson, W. I., Jr., Easter, R. C., Zaveri, R. A., Barnard, J. C., Chapman, E. G., et al. (2006). Evolution of ozone, particulates, and aerosol direct radiative forcing in the vicinity of Houston using a fully coupled meteorology-chemistry-aerosol model. *Journal of Geophysical Research D*, *111*(D21). https://doi.org/10.1029/2005JD006721

Flamant, C., Chaboureau, J.-P., Parker, D. J., Taylor, C. M., Cammas, J. P., Bock, O., et al. (2007). Airborne observations of the impact of a convective system on the planetary boundary layer thermodynamics and aerosol distribution in the intertropical discontinuity region of the West African monsoon. *Quarterly Journal of the Royal Meteorological Society*, *133*, 1175–1189. https://doi.org/10.1002/qj.97

Fonseca, R., Temimi, M., Thota, M. S., Nelli, N. R., Weston, M. J., Suzuki, K., et al. (2020). On the analysis of the performance of WRF and NICAM in a hyperarid environment. *Weather and Forecasting*, *35*(3), 891–919. https://doi.org/10.1175/WAF-D-19-0210.1

Gentine, P., Garelli, A., Park, S.-B., Nie, J., Torri, G., & Kuang, Z. (2016). Role of surface heat fluxes underneath cold pools. *Geophysical Research Letters*, *43*, 874–883. https://doi.org/10.1002/2015GL067262

Ginoux, P., Chin, M., Tegen, I., Prospero, J. M., Holben, B., Dubovik, O., & Lin, S.-J. (2001). Sources and distributions of dust aerosols simulated with the GOCART model. *Journal of Geophysical Research D*, *106*, 20255–20273. https://doi.org/10.1029/2000JD000053

Goudie, A. S. (2014). Desert dust and human health disorders. *Environment International*, *63*, 101–113. https://doi.org/10.1016/j.envint.2013.10.011

Grant, L. D., & van den Heever, S. C. (2015). Cold pool and precipitation responses to aerosol loading: Modulation by dry layers. *Journal of the Atmospheric Sciences*, *72*, 1398–1408. https://doi.org/10.1175/JAS-D-14-0260.1

Grant, L. D., & van den Heever, S. C. (2016). Cold pool dissipation. *Journal of Geophysical Research - D: Atmospheres*, *121*, 1138–1155. https://doi.org/10.1002/2015JD023813

Grant, L. D., & van den Heever, S. C. (2018). Cold pool-land surface interactions in a dry continental environment. *Journal of Advances in Modeling Earth Systems*, *10*, 1513–1526. https://doi.org/10.1029/2018MS001323

Grell, G. A., Peckham, S. E., Schmitz, R., McKeen, S. A., Frost, G., Skamarock, W. C., & Eder, B. (2005). Fully coupled "online" chemistry within the WRF model. *Atmospheric Environment*, *39*, 6957–6975. https://doi.org/10.1016/J.ATMOSENV10.1016/j.atmosenv.2005.04.027

Hansell, R. A., Tsay, S. C., Ji, Q., Hsu, N. C., Jeong, M. J., Wang, S. H., et al. (2010). An assessment of the surface longwave direct radiative effect of airborne Saharan dust during the NAMMA field campaign. *Journal of the Atmospheric Sciences*, *67*, 1048–1065. https://doi.org/10.1175/2009JAS3257.1

Heikenfeld, M., Marinescu, P. J., Christensen, M., Watson-Parris, D., Senf, F., van den Heever, S. C., & Stier, P. (2019). Tobac 1.2: Towards a flexible framework for tracking and analysis of clouds in diverse datasets. *Geoscientific Model Development*, *12*, 4551–4570. https://doi.org/10.5194/gmd-12-4551-2019

Heinold, B., Tegen, I., Schepanski, K., & Hellmuth, O. (2008). Dust radiative feedback onSaharan boundary layer dynamics and dust mobilization. *Geophysical Research Letters*, *35*, L20817. https://doi.org/10.1029/2008GL035319

Heinold, B., Helmert, J., Hellmuth, O., Wolke, R., Ansmann, A., Marticorena, B., et al. (2007). Regional modeling of Saharan dust events using LM-MUSCAT: Model description and case studies. *Journal of Geophysical Research*, *112*, D11204. https://doi.org/10.1029/2006JD007443

Heinold, B., Knippertz, P., Marsham, J. H., Fiedler, S., Dixon, N. S., Schepanski, K., et al. (2013). The role of deep convection and nocturnal low-level jets for dust emission in summertime West Africa: Estimates from convection-permitting simulations. *Journal of Geophysical Research D: Atmospheres*, *118*, 4385–4400. https://doi.org/10.1002/jgrd.50402

Heintzenberg, J. (2009). The SAMUM-1 experiment over Southern Morocco: Overview and introduction. *Tellus B: Chemical and Physical Meteorology*, *61*, 2–11. https://doi.org/10.1111/j.1600-0889.2008.00403.x

Hoshyaripour, G. A., Bachmann, V., Förstner, J., Steiner, A., Vogel, H., Wagner, F., et al. (2019). Effects of particle nonsphericity on dust optical properties in a forecast system: Implications for model-observation comparison. *Journal of Geophysical Research: Atmosphere*, *124*, 7164–7178. https://doi.org/10.1029/2018jd030228

Huang, Q., Marsham, J. H., Tian, W., Parker, D. J., & Garcia-Carreras, L. (2018). Large-eddy simulation of dust-uplift by a haboob density current. *Atmospheric Environment*, *179*, 31–39. https://doi.org/10.1016/j.atmosenv.2018.01.048

Huang, Y., Adebiyi, A. A., Formenti, P., & Kok, J. F. (2021). Linking the different diameter types of aspherical desert dust indicates that models underestimate coarse dust emission. *Geophysical Research Letters*, *48*, e2020GL092054. https://doi.org/10.1029/2020gl092054

Iacono, M. J., Delamere, J. S., Mlawer, E. J., Shephard, M. W., Clough, S. A., & Collins, W. D. (2008). Radiative forcing by long-lived greenhouse gases: Calculations with the AER radiative transfer models. *Journal of Geophysical Research*, *113*, D13103. https://doi.org/10.1029/2008JD009944

Jacobson, M. Z., & Kaufman, Y. J. (2006). Wind reduction by aerosol particles. *Geophysical Research Letters*, *33*, L24814. https://doi.org/10.1029/2006GL027838

Jiang, H., & Feingold, G. (2006). Effect of aerosol on warm convective clouds: Aerosol-cloud surface flux feedbacks in a new coupled large eddy model. *Journal of Geophysical Research*, *111*, D01202. https://doi.org/10.1029/2005JD006138

Journet, E., Balkanski, Y., & Harrison, S. P. (2014). A new data set of soil mineralogy for dust-cycle modeling. *Atmospheric Chemistry and Physics*, *14*, 3801–3816. https://doi.org/10.5194/acp-14-3801-2014

Knippertz, P., & Todd, M. C. (2012). Mineral dust aerosols over the Sahara: Meteorological controls on emission and transport and implications for modeling. *Reviews of Geophysics*, *50*, 140–147. https://doi.org/10.1029/2011RG000362

Knippertz, P., Trentmann, J., & Seifert, A. (2009). High-resolution simulations of convective cold pools over the northwestern Sahara. *Journal of Geophysical Research*, *114*, D08110. https://doi.org/10.1029/2008JD011271

Kok, J. F., Ridley, D. A., Zhou, Q., Miller, R. L., Zhao, C., Heald, C. L., et al. (2017). Smaller desert dust cooling effect estimated from analysis of dust size and abundance. *Nature Geoscience*, *10*(4), 274–278. https://doi.org/10.1038/ngeo2912

Kurowski, M. J., Suselj, K., Grabowski, W. W., & Teixeira, J. (2018). Shallow-to-deep transition of continental moist convection: Cold pools, surface fluxes, and mesoscale organization. *Journal of the Atmospheric Sciences*, *75*(12), 4071–4090. https://doi.org/10.1175/JAS-D-18-0031.1

Largeron, Y., Guichard, F., Bouniol, D., Couvreux, F., Kergoat, L., & Marticorena, B. (2015). Can we use surface wind fields from meteorological reanalyses for Sahelian dust emission simulations? *Geophysical Research Letters*, *42*, 2490–2499. https://doi.org/10.1002/2014GL062938

Lemaître, C., Flamant, C., Cuesta, J., Raut, J.-C., Chazette, P., Formenti, P., & Pelon, J. (2010). Radiative heating rates profiles associated with a springtime case of Bodélé and Sudan dust transport over West Africa. *Atmospheric Chemistry and Physics*, *10*, 8131–8150. https://doi.org/10.5194/acp-10-8131-2010

Leys, J. F., Heidenreich, S. K., Strong, C. L., McTainsh, G. H., & Quigley, S. (2011). PM10 concentrations and mass transport during "Red Dawn" – Sydney 23 September 2009. *Aeolian Research*, *3*, 327–342. https://doi.org/10.1016/j.aeolia.2011.06.003

Li, L., Mahowald, N. M., Miller, R. L., Pérez García-Pando, C., Klose, M., Hamilton, D. S., et al. (2021). Quantifying the range of the dust direct radiative effect due to source mineralogy uncertainty. *Atmospheric Chemistry and Physics*, *21*, 3973–4005. https://doi.org/10.5194/acp-21-3973-2021

Liu, C., & Moncrieff, M. W. (2000). Simulated density currents in idealized stratified environments. *Monthly Weather Review*, *128*, 1420–1437. https://doi.org/10.1175/1520-0493(2000)12810.1175/1520-0493(2000)128<1420:sdciis>2.0.co;2

Liu, L., Huang, X., Ding, A., & Fu, C. (2016). Dust-induced radiative feedbacks in north China: A dust storm episode modeling study using WRF-Chem. *Atmospheric Environment*, *129*, 43–54. https://doi.org/10.1016/j.atmosenv.2016.01.019

Mahowald, N., AlbaniKok, S. J. F., Engelstaeder, S., Scanza, R., Ward, D. S., & Flanner, M. G. (2014). The size distribution of desert dust aerosols and its impact on the Earth system. *Aeolian Research*, *15*, 53–71. https://doi.org/10.1016/j.aeolia.2013.09.002

Mallet, M., Tulet, P., Serça, D., Solmon, F., Dubovik, O., Pelon, J., et al. (2009). Impact of dust aerosols on the radiative budget, surface heat fluxes, heating rate profiles and convective activity over West Africa during March 2006. *Atmospheric Chemistry and Physics*, *9*, 7143–7160. https://doi.org/10.5194/acp-9-7143-2009

Marsham, J. H., Parker, D. J., Todd, M. C., Banks, J. R., Brindley, H. E., Garcia-Carreras, L., et al. (2016). The contrasting roles of water and dust in controlling daily variations in radiative heating of the summertime Saharan heat low. *Atmospheric Chemistry and Physics*, *16*, 3563–3575. https://doi.org/10.5194/acp-16-3563-2016

Meloni, D., Junkermann, W., di Sarra, A., Cacciani, M., De Silvestri, L., Di Iorio, T., et al. (2015). Altitude-resolved shortwave and longwave radiative effects of desert dust in the Mediterranean during the GAMARF campaign: Indications of a net daily cooling in the dust layer. *Journal of Geophysical Research D*, *120*, 3386–3407. https://doi.org/10.1002/2014JD022312

Membery, D. A. (1985). A gravity-wave haboob? *Weather*, *40*, 214–221. https://doi.org/10.1002/j.1477-8696.1985.tb06877.x
Middleton, N. J. (2017). Desert dust hazards: A global review. *Aeolian Research*, *24*, 53–63. https://doi.org/10.1016/j.aeolia.2016.12.001
Middleton, N., & Kang, U. (2017). Sand and dust storms: Impact mitigation. *Sustainability*, *9*, 1053. https://doi.org/10.3390/su9061053
Miller, R. L., Perlwitz, J., & Tegen, I. (2004). Feedback upon dust emission by dust radiative forcing through the planetary boundary layer. *Journal of Geophysical Research*, *109*, D24209. https://doi.org/10.1029/10.1029/2004JD004912
Miller, S. D., Kuciauskas, A. P., Liu, M., Ji, Q., Reid, J. S., Breed, D. W., et al. (2008). Haboob dust storms of the southern Arabian Peninsula. *Journal of Geophysical Research D*, *113*, D01202. https://doi.org/10.1029/2007JD008550
Miller, S. D., Grasso, L. D., Bian, Q., Kreidenweis, S. M., Dostalek, J. F., Solbrig, J. E., et al. (2019). A tale of two dust storms: Analysis of a complex dust event in the Middle East. *Atmospheric Measurement Techniques*, *12*, 5101–5118. https://doi.org/10.5194/amt-12-5101-2019
Mishra, A. K., Klingmueller, K., Fredj, E., Lelieveld, J., Rudich, Y., & Koren, I. (2014). Radiative signature of absorbing aerosol over the eastern Mediterranean basin. *Atmospheric Chemistry and Physics*, *14*, 7213–7231. https://doi.org/10.5194/acp-14-7213-2014
Moncrieff, M. W., & Liu, C. (1999). Convection initiation by density currents: Role of convergence, shear, and dynamical organization. *Monthly Weather Review*, *127*, 2455–2464. https://doi.org/10.1175/1520-0493(1999)127<2455:cibdcr>2.0.co;2
Morrison, H., Thompson, G., & Tatarskii, V. (2009). Impact of cloud microphysics on the development of trailing stratiform precipitation in a simulated squall line: Comparison of one- and two-moment schemes. *Monthly Weather Review*, *137*, 991–1007. https://doi.org/10.1175/2008MWR2556.1
Morrison, H., Curry, J. A., & Khvorostyanov, V. I. (2005). A new double-moment microphysics parameterization for application in cloud and climate models. Part I: Description. *Journal of the Atmospheric Sciences*, *62*, 1665–1677. https://doi.org/10.1175/JAS3446.1
Nakanishi, M., & Niino, H. (2006). An improved Mellor–Yamada level-3 model: Its numerical stability and application to a regional prediction of advection fog. *Boundary-Layer Meteorology*, *119*, 397–407. https://doi.org/10.1007/s10546-005-9030-8
Nakanishi, M., & Niino, H. (2009). Development of an improved turbulence closure model for the atmospheric boundary layer. *Journal of the Meteorological Society of Japan. Ser. II*, *87*, 895–912. https://doi.org/10.2151/jmsj.87.895
National Centers for Environmental Prediction/National Weather Service/NOAA/U.S. Department of Commerce: NCEP FNL Operational Model Global Tropospheric Analyses, continuing from July 1999 (2000). Research Data Archive at the National Center for Atmospheric Research,Computational and Information Systems Laboratory. https://doi.org/10.5065/D6M043C6
National Centers for Environmental Prediction/National Weather Service/NOAA/U.S. Department of Commerce: NCEP GDAS/FNL 0.25 Degree Global Tropospheric Analyses and Forecast Grids (2015). Research data archive at the national center for atmospheric Research, Computational and Information Systems Laboratory. https://doi.org/10.5065/D65Q4T4Z
Nelli, N. R., Temimi, M., Fonseca, R. M., Weston, M. J., Thota, M. S., Valappil, V. K., et al. (2020). Impact of roughness length on WRF simulated land-atmosphere interactions over a hyper-arid region. *Earth and Space Science*, *7*, e2020EA001165. https://doi.org/10.1029/2020EA001165
Niu, G.-Y., Yang, Z.-L., Mitchell, K. E., Chen, F., Ek, M. B., Barlage, M., et al. (2011). The community Noah land surface model with multiparameterization options (Noah-MP): 1. Model description and evaluation with local-scale measurements. *Journal of Geophysical Research D*, *116*, D12109. https://doi.org/10.1029/2010JD015139
Pantillon, F., Knippertz, P., Marsham, J. H., & Birch, C. E. (2015). A parameterization of convective sust storms for models with mass-flux convection schemes. *Journal of the Atmospheric Sciences*, *72*, 2545–2561. https://doi.org/10.1175/JAS-D-14-0341.1
Pantillon, F., Knippertz, P., Marsham, J. H., Panitz, H., & Bischoff-Gauss, I. (2016). Modelling haboob dust storms in large-scale weather and climate models. *Journal of Geophysical Research D: Atmospheres*, *121*, 2090–2109. https://doi.org/10.1002/2015JD024349
Pérez, C., Nickovic, S., Pejanovic, G., Baldasano, J. M., & Özsoy, E. (2006). Interactive dust radiation modeling: A step to improve weather forecasts. *Journal of Geophysical Research D*, *111*, D16206. https://doi.org/10.1029/2005JD006717
Peris-Ferrús, C., Gómez-Amo, J. L., Marcos, C., Freile-Aranda, M. D., Utrillas, M. P., & Martínez-Lozano, J. A. (2017). Heating rate profiles and radiative forcing due to a dust storm in the Western Mediterranean using satellite observations. *Atmospheric Environment*, *160*, 142–153. https://doi.org/10.1016/j.atmosenv.2017.04.023
Perlwitz, J., Tegen, I., & Miller, R. L. (2001). Interactive soil dust aerosol model in the GISS GCM: 1. Sensitivity of the soil dust cycle to radiative properties of soil dust aerosols. *Journal of Geophysical Research*, *106*(D16), 18167–18192. https://doi.org/10.1029/2000JD900668
Pope, R. J., Marsham, J. H., Knippertz, P., Brooks, M. E., & Roberts, A. J. (2016). Identifying errors in dust models from data assimilation. *Geophysical Research Letters*, *43*, 9270–9279. https://doi.org/10.1002/2016GL070621
Prospero, J. M., Ginoux, P., Torres, O., Nicholson, S. E., & Gill, T. E. (2002). Environmental characterization of global sources of atmospheric soil dust identified with the Nimbus 7 Total Ozone Mapping Spectrometer (TOMS) absorbing aerosol product. *Reviews of Geophysics*, *40*, 1002. https://doi.org/10.1029/2000RG000095
Purdom, J. F. W. (1982). Subjective interpretation of geostationary satellite data for nowcasting. In K. Browning (Ed.), *Nowcasting* (pp. 149–156). Academic Press .
Quijano, A. L., Sokolik, I. N., & Toon, O. B. (2000). Radiative heating rates and direct radiative forcing by mineral dust in cloudy atmospheric conditions. *Journal of Geophysical Research*, *105*(D10), 12207–12219. https://doi.org/10.1029/2000JD900047
Rémy, S., Benedetti, A., Bozzo, A., Haiden, T., Jones, L., Razinger, M., et al. (2015). Feedbacks of dust and boundary layer meteorology during a dust storm in the eastern Mediterranean. *Atmospheric Chemistry and Physics*, *15*, 12909–12933. https://doi.org/10.5194/acp-15-12909-2015
Roberts, A. J., & Knippertz, P. (2012). Haboobs: Convectively generated dust storms in West Africa. *Weather*, *67*, 311–316. https://doi.org/10.1002/wea.1968
Roberts, A. J., & Knippertz, P. (2014). The formation of a large summertime Saharan dust plume: Convective and synoptic-scale analysis. *Journal of Geophysical Research D*, *119*, 1766–1785. https://doi.org/10.1002/2013JD020667
Rotunno, R., Klemp, J. B., & Weisman, M. L. (1988). A theory for strong, long-lived squall lines. *Journal of the Atmospheric Sciences*, *45*, 463–485. https://doi.org/10.1175/1520-0469(1988)045<0463:atfsll>2.0.co;2
Saleeby, S. M., van den Heever, S. C., Bukowski, J., Walker, A. L., Solbrig, J. E., Atwood, S. A., et al. (2019). The influence of simulated surface dust lofting and atmospheric loading on radiative forcing. *Atmospheric Chemistry and Physics*, *19*, 10279–10301. https://doi.org/10.5194/acp-19-10279-2019
Schepanski, K., Tegen, I., Laurent, B., Heinold, B., & Macke, A. (2007). A new Saharan dust source activation frequency map derived from MSG-SEVIRI IR-channels. *Geophysical Research Letters*, *34*, L18803. https://doi.org/10.1029/2007GL030168
Seigel, R. B., & van den Heever, S. C. (2012a). Dust lofting and ingestion by supercell storms. *Journal of the Atmospheric Sciences*, *69*, 1453–1473. https://doi.org/10.1175/JAS-D-11-0222.1
Seigel, R. B., & van den Heever, S. C. (2012b). Simulated density currents beneath embedded stratified layers. *Journal of the Atmospheric Sciences*, *69*, 2192–2200. https://doi.org/10.1175/JAS-D-11-0255.1

Seigel, R. B., van den Heever, S. C., & Saleeby, S. M. (2013). Mineral dust indirect effects and cloud radiative feedbacks of a simulated idealized nocturnal squall line. *Atmospheric Chemistry and Physics*, *13*, 4467–4485. https://doi.org/10.5194/acp-13-4467-2013

Skamarock, W. C., Klemp, J. B., Dudhia, J. O. G. D., & Barker, D. M. (2008). A description of the Advanced Research WRF version 3 (No. NCAR/TN-4751+STR). *NCAR Tech*. https://doi.org/10.5065/D68S4MVH

Slingo, A., Ackerman, T. P., Allan, R. P., Kassianov, E. I., McFarlane, S. A., Robinson, G. J., et al. (2006). Observations of the impact of a major Saharan dust storm on the atmospheric radiation balance. *Geophysical Research Letters*, *33*, L24817. https://doi.org/10.1029/2006GL027869

Sprigg, W. A. (2016). Dust storms, human health and a global early warning system. In S. Steinberg, & W. Sprigg (Eds.), *Extreme Weather, Health, and Communities. Extreme weather and society* (pp. 59–87). Springer International Publishing. https://doi.org/10.1007/978-3-319-30626-1_4

Takemi, T. (2005). Explicit simulations of convective-scale transport of mineral dust in severe convective weather. *Journal of the Meteorological Society of Japan*, *83A*, 187–203. https://doi.org/10.2151/jmsj.83A.187

Tegen, I., & Lacis, A. A. (1996). Modeling of particle size distribution and its influence on the radiative properties of mineral dust aerosol. *Journal of Geophysical Research*, *101*, 19237–19244. https://doi.org/10.1029/95JD03610

Thorpe, A. J., Miller, M. J., & Moncrieff, M. W. (1982). Two-dimensional convection in non-constant shear: A model of mid-latitude squall lines. *Quarterly Journal of the Royal Meteorological Society*, *108*, 739–762. https://doi.org/10.1002/qj.49710845802

Tompkins, A. M. (2001). Organization of tropical convection in low vertical wind shears: The role of cold pools. *Journal of the Atmospheric Sciences*, *58*, 1650–1672. https://doi.org/10.1175/1520-0469(2001)058<1650:ootcil>2.0.co;2

Torri, G., Kuang, Z., & Tian, Y. (2015). Mechanisms for convection triggering by cold pools. *Geophysical Research Letters*, *42*, 1943–1950. https://doi.org/10.1002/2015GL063227

Tulet, P., Crahan-Kaku, K., Leriche, M., Aouizerats, B., & Crumeyrolle, S. (2010). Mixing of dust aerosols into a mesoscale convective system: Generation, filtering and possible feedbacks on ice anvils. *Atmospheric Research*, *96*, 302–314. https://doi.org/10.1016/j.atmosres.2009.09.011

Uno, I., Wang, Z., Chiba, M., Chun, Y. S., Gong, S. L., Hara, Y., et al. (2006). Dust model intercomparison (DMIP) study over Asia: Overview. *Journal of Geophysical Research*, *111*, D12213. https://doi.org/10.1029/2005JD006575

van den Heever, S. C., Carrio, G. G., Cotton, W. R., DeMott, P. J., & Prenni, A. J. (2006). Impacts of nucleating aerosol on Florida storms. Part I: Mesoscale simulations. *Journal of the Atmospheric Sciences*, *63*, 1752–1775. https://doi.org/10.1175/JAS3713.1

Vescio, M. D., & Johnson, R. H. (1992). The wind response to transient mesoscale pressure fields associated with squall lines. *Monthly Weather Review*, *120*, 1837–1850. https://doi.org/10.1175/1520-0493(1992)120<1837:tswrtt>2.0.co;2

Walker, A. L., Liu, M., Miller, S. D., Richardson, K. A., & Westphal, D. L. (2009). Development of a dust source database for mesoscale forecasting in southwest Asia. *Journal of Geophysical Research*, *114*, D18207. https://doi.org/10.1029/2008JD011541

Weaver, J. F., & Nelson, S. P. (1982). Multiscale aspects of thunderstorm gust fronts and their effects on subsequent storm development. *Monthly Weather Review*, *110*, 707–718. https://doi.org/10.1175/1520-0493(1982)110<0707:maotgf>2.0.co;2

Weisman, M. L., & Rotunno, R. (2004). "A theory for strong, long-lived squall lines" revisited. *Journal of the Atmospheric Sciences*, *61*(4), 361–382. https://doi.org/10.1175/1520-0469(2004)061<0361:atfsls>2.0.co;2

Wilson, J. W., & Schreiber, W. E. (1986). Initiation of convective storms at radar-observed boundary-layer convergence lines. *Monthly Weather Review*, *114*, 2516–2536. https://doi.org/10.1175/1520-0493(1986)114<2516:iocsar>2.0.co;2

Yang, Z.-L., Niu, G.-Y., Mitchell, K. E., Chen, F., Ek, M. B., Barlage, M., et al. (2011). The community Noah land surface model with multiparameterization options (Noah-MP): 2. Evaluation over global river basins. *Journal of Geophysical Research*, *116*, D12110. https://doi.org/10.1029/2010JD015140

Zhang, K., & Wang, X. (1997). Investigation report and some thinking on strong sand storm in Northwest China, May 5, 1993. *Journal of Beijing Forestry University*, *19*, 1.